8-2020

Lead Free Piezoelectric and Triboelectric Energy Film for Energy Harvesting and Sensory Applications

Abu Musa Abdullah
The University of Texas Rio Grande Valley

LEAD FREE PIEZOELECTRIC AND TRIBOELECTRIC ENERGY FILM FOR ENERGY HARVESTING AND SENSORY APPLICATIONS

A Thesis

by

ABU MUSA ABDULLAH

Submitted to the Graduate College of
The University of Texas Rio Grande Valley
In partial fulfillment of the requirements for the degree of

MASTER OF SCIENCE IN ENGINEERING

August 2020

Major Subject: Mechanical Engineering

LEAD FREE PIEZOELECTRIC AND TRIBOELECTRIC ENERGY FILM FOR ENERGY HARVESTING AND SENSORY APPLICATIONS.

A Thesis
by
ABU MUSA ABDULLAH

COMMITTEE MEMBERS

Dr. Mohammed Jasim Uddin
Chair of Committee

Dr. Horacio Vasquez
Committee Member

Dr. Yingchen Yang
Committee Member

August 2020

ABSTRACT

Abdullah, Abu Musa, Lead Free Piezoelectric and Triboelectric Energy Film for Energy Harvesting and Sensory Applications Master of Science in Engineering (MSE), August 2020, 87 pp., 17 figures, 160 references

In recent times, Triboelectricity and Piezoelectricity has been widely used for utilizing mechanical energy from ambient environment. Scientists are focusing towards developing advanced material composites for utilizing piezoelectricity and triboelectricity for energy harvesting and sensory applications. This work includes two projects regarding the application of lead free piezoelectric and triboelectric energy for energy harvesting and sensory applications. Human motion has been attributed as a source of mechanical energy to drive electronic devices and sensors through Triboelectric Nanogenerator (TENG). Based on the principles of single electrode TENG, we have developed a Triboelectricity based Stepping and Tapping Energy Case (TESTEC) which magnifies the prospect to power touch electronic devices by utilizing finger tapping and stepping motion. This novel case was constructed with two single electrode TENG operating through the triboelectric mechanism between human skin and Polyethylene terephthalate(PET) film on the front part and Nitrile Butadiene Rubber(NBR) and PET film on the back part. This cost effective device was further tested by attaching with a cell phone at variable load frequency, airgap and finger combinations where the output response increased with the increased frequencies (60 to 240 BPM) and air gap (1cm to 5cm). Maximum output

voltages of 14.8 V and 50.8 V were obtained for the front and back parts, respectively. Besides, maximum output powers were observed to be 3.78 W/m^2 at 0.46 MΩ and 6.21 W/m^2 at 1.02 MΩ, respectively. Also, the device was tested by integrating with conventional electronic components including capacitors, bridge rectifiers and 15 LEDs. The TESTEC can be a self sustainable way to power touch electronic devices which can reudce the necessity to charge electronics devices in the conventional way. In the second part of this work, a Potassium Sodium Niobate (KNN) nanocube based energy film (EF) has been developed for utilizing mechanical Energy through triboelectric and piezoelectric mechanism. The KNN particles were synthesized using wet ball milling technique incorporated into Polyvinylidene Difluoride (PVDF) matrix and along with Multi Wall Carbon Nanotube (MWCNT). The film was used to develop a Piezoelectric Nanogenerator (PENG) with Copper electrodes. The piezoelectric output of the film was further tested with Copper electrodes at variable tapping frequency (60 BPM to 240 BPM) and Pressure (10 PSI to 40 PSI). The open circuit voltage increased with the increase of both tapping frequency and pressure. The maximum piezoelectric output voltage was observed to be 35.3 V while the maximum current was noted as 15.8 µA. The films also showed unique output signals for different types of finger motions. The film was further utilized to build a Piezo-triboelectric hybrid nanogenerator to check its hybrid performance. The maximum output was observed to be 54.1 V and 29.4 µA in this case. This experiment endorsed the potential of the KNN based energy film for multifunctional application like force, pressure and motion sensing as well as lead free energy harvesting.

DEDICATION

Thanks to the almighty. My Journey at UTRGV for the Master's studies would not have been possible without the love and support of my family and friends. I dedicate this work to my mother Farida Yeasmin, my Father Md. Kabir Hossain, my wife Fatema Tuz Zohra and my beautiful babygirl- whom I am eagered to meet soon in this World. They have been the main base of my journey so far.

ACKNOWLEDGEMENT

First of all I would like to acknowledge my supervisor, Dr. M. Jasim Uddin for his support and guidance. His continous mentorship along with his excellent vision and expertise is the field of Materials Science really motivated in my journey so far. I am very proud to be a member of Photonics and Energy Research Laboratory under his supervision. Besides, I would also like to mention about my fellow collegues who has been a wonderful support so for. Particularly, I would talk about Muhtashim Ul Karim Sadaf- who has a tromendous vision and dedication towards his work. Besides, I would thank my other team members- Alejandro Flores, Damian Zamora and Julian Escober who have been a tromendous fellas to work with. Also, I am very thankful to Istiak Hussain and Aminur Rashid Chowdhury for their excellent support in the initial stage of my journey. It would have been very tough without both of them. Correspondingly, I thank my other lab members- Isaac Martinez, Carolina Olivares, Farzana Tasnim and SK Ali Zaker Shawon for their help. I also thank the new members- Haimanti Majumder and Valeria S Vega and wish them best of luck. I can not forget the contribution of Bangladeshi Community throughout this journey. Specially, I would like to mention about Abdullah Al Masum- who has been like my brother providing huge support throughout this journey. Besides, two other fellas were really there for me- Al Mazedur Rahman Prince and Prosanto Biswas. Likewise I would express my humble grattitude towards the members of the community. Specially, Sayeed Wadud, Abdullah Al Noman, Md. Ruhul Amin, Muniruzzaman

Chowdhury, Hasan Anowar, Sadia Sharmin, Md. Fazle Rabby, Fatema Hamim, Wasif Zaman Jitu, Afsana Akter Moushumi, Mostafa Meraj Pasha, Taeba Tuba, Mirza Aditto Billah (Panda), Apu Deb, Saumik Sakib, Abdullah Al Tusher, Aneek Salman, Al Amin, Md. Shakhawat Hossain and so on. I am grateful to the Department of Mechanical Engineering-UTRGV and The Graduate College-UTRGV. Then, I would like to humbly express my grattidue towards all the faculties of my department. Specially to mu co-supervisor Dr. Horacio Vasquez and my thesis comitte member Dr. Yingchen Yang. Besides, I also thank Dr. Rogelio Benitez, Dr. Noe Vargas, Dr. Philip Park and Mr. John Pamelton. One faculty I would like to specially mention about- Dr. Karen Lozano; who has inspired me a lot. She has been one of the moticvational and supporting personalties I have ever seen. I am very thankful Dr. Parwender Grewal as well. Dr. Grewal is an strong support to all the graduate students at UTRGV. Wihtout his visionary step, it would have been impossible to work as a PGRA. Next, I would like to mention my beautiful wife- Fatema Tuz Zohra who is currently holding my princess inside. They are one my biggest reasons to smile. I also thank my father in law Mr. Abdul Mottaleb, mother in law Mrs Sufia Akhter and sister in law Umme Anika Tabassum. Finally and most importantly, I would like to express my grattitude towards my mother Farida Yeasmin and my father Dr. Md. Kabir Hossain. My father has always motivted me to be honest and hardworking. My mother has been my ultimate support and a strong force of my breathig who has always believed on me. I could no do anything without them. Thanks to the almighty again.

TABLE OF CONTENTS

Page

LIST OF FIGURES

Page

CHAPTER I

INTRODUCTION

Energy deficiency has become a worldwide issue in the twenty-first century[1]. Over the past few decades, intensive efforts have been made to hunt for alternative energy sources. because of the threats represented by the fluctuation of petroleum fuel costs, the danger of climate change and predicted consumption of non-sustainable fuel sources [2,3]. This demand of energy will be doubled by the end of 2035 which is also expected to increase in an order of 1 GW per day till 2050 [4,5]. However, due to the limitation of natural resource and environmental pollution caused by energy production and consumption, experts are focusing towards sustainable development and green energy for meeting the energy demand for today and tomorrow [3,6–8]. These crisis has become the motivation for the fabrication of high-yield materials to scavenge energy from the environment and sense environmental stresses [4].The rapid progress of nanotechnology has received widespread attention by encompassing a continuous study and developing materials with improved properties revealing breakthroughs [3].To fulfill these criteria, Wang *et al*. [9] made a nanogenerator based on the piezoelectric effect, which was a revolutionary invention towards the goal of mechanical harvesting energy in 2006. The piezoelectric effect was discovered by Nobel laureates Pierre and Jacques Curie in 1880.[10] Later in 2012, the idea of a nanogenerator utilizing triboelectric property of material

with low cost, high power density, lightweight, good flexibility, and excellent efficiency has been introduced by Dr. Wang and his group, naming Triboelectric Nanogenerator (TENG) [11,12]. Piezoelectric, triboelectric and combination of piezoelectric-triboelectric nanogenerators have spearheaded the research in harvesting ambient mechanical energy over the last decade [13,14]. Energy harvesting from human movements have led to a variety of inventions like self-powered devices, sustainable wearable devices, sensors and actuators [15–18]. This shows the potential that is held by these nanogenerators in the path towards sustainable power sources development.

Piezoelectric devices are being used for their thin, flexible, and in some cases, mechanically stretchable structure [10,19]. This allows them to be suitable for mounting on any type of surface. Developments in materials studies and manufacturing has yielded piezoelectric devices from organic materials that can produce a maximum open-circuit voltage of ~80 V and a short-circuit current of ~300 μA without costly operations such as poling [20]. Triboelectric nanogenerators have also shown superior open-circuit voltage and current. It has been seen that a triboelectric nanogenerator can produce open-circuit voltage of ~4000V and short-circuit current of ~0.12A [20–22]. Besides, The output power density and energy conversion efficiency of TENG can be as high as 500Wcm^{-2} and 85% [23–25]. Combination between triboelectric and piezoelectric materials creates hybrid nanogenerators that can produce high and efficient output with single source of external force [26,27]. In a recent work by Jung *et al,* a piezoelectric-triboelectric hybrid nanogenerator was constructed that can reach an open-circuit voltage of ~370V and a current density of ~12 μA/cm^2 [20]. Furthermore, These devices are very effective in charging capacitors and very sensitive to forces [4,28]. These characteristics show the

potential of these devices in sensory applications in addition to the mechanical energy harvesting.

It is very important to choose appropriate material for the effective utilization of the piezoelectric and triboelectric effect [19,29] Polyvinylidene fluoride (PVDF) is one of the most versatile piezoelectric polymers till now due to lower density, higher flexibility, lower resistance, and higher piezoelectric voltage.[30,31] PVDF can also work as a tribo-negative polymer. [32] PVDF has several crystalline polymorphs (α, β, γ, δ and ε) depending on the chain conformation[33] Amid all crystalline phases, β and γ are of high priority because of its spontaneous polarization and piezoelectric sensitivity. Several methods are used to induce β phase in PVDF[34]. The stretching, annealing or poling is one of the processes to transform PVDF from α to β phase.[35] Yu *et al*. [36], and Kim *et al*. [37] confirmed that the use of carbon nanotubes (CNTs) as filler in the PVDF matrix that leads to a relevant increase in the β-phase content. Moreover, Multi Wall Carbon Nano Tube (MWCNT) boosts the conductivity of composites by creating a 3D network of conductive MWCNT in the polymer matrix, which ease off electron flow during triboelectric/piezoelectric actions.[4] Kim *et al*. [38] proposed the triboelectric performance of PVDF composites with MWCNTs. Chowdhury *et al*.[39] also demonstrated a tribo-piezo hybrid nanogenerator with PVDF/MWCNT/Li-ZnO as the piezoelectric component and PTFE/PDMS as the triboelectric component.

PVDF composite incorporating various kinds of inorganic materials ZnO, $Pb(Zr,Ti)O_3$(PZT), $BaTiO_3$(BTO), $(K,Na)NbO_3$(KNN), $ZnSnO_3$, GaN, MoS_2 nanoparticles have been explored in the past to fabricate more efficient piezoelectric energy harvester. [40] PZT is a commonly utilized piezoelectric ceramic material with active materials for mechanical to electrical energy conversions, like high piezoelectric voltage and dielectric constants, than other

semiconductor types of piezoelectric materials.[41] Park *et al*. [42], showed a flexible piezoelectric PZT thin film nanogenerator on plastic substrates. Lu *et al*. [43] also discussed multi-material piezoelectric fibers fabricated from perovskite ceramic NPs (BT/PZT)-PVDF and CNT-PVDF composites via fiber drawing. However, due to the high toxicity of PZT, PZT-PVDF fibers are probably not suitable for wearable applications[44]. Nevertheless, the low conductivity of PZT is not ideal for output performance.[40] Synthesizing low-dimensional, single-crystal, lead-free piezoelectric nanomaterials can mitigate these issues. [19] Among the available materials, $ZnSnO_3$, a lead-free multifunctional piezoelectric nanomaterials, has attracted considerable interest lately and has great potential in applications in numerous fields. [40] Apart from that, especially, alkaline niobates, based on the perovskite-type oxide(K,Na) NbO_3, have also been in discussion in recent days as promising lead free piezoelectric ceramics.[45] [46] Teka *et at*. [47] portrayed his research work with potassium sodium niobate, $(Na,K)NbO_3$ (KNN) as a nano piezoelectric filler, because of their large piezoelectric response, ferroelectric properties, and higher curie temperature (>400°C) and also is suitable when a low cost and lightweight device is the requirement. KNN is well known as a lead-free energy material which can be used with other functional materials for making piezoelectric coposites [48,49]. However, the performance of KNN based nanogenerator still requires higher output for real life and industrial applications. For instance, Bairagi *et al*, developed piezoelectric nanogenerator based on KNN and PVDF which showed a maximum output of 23.24 V and 18 μA [50]. Nevertheless, the triboelectric property of PVDF has not been utilized in these works yet.

Modern electronic devices like cellphones, tablets, calculators *etc*. are required to be small, lightweight and efficient in order to make them portable and competitive in the consumer market [51]. Electronic devices are getting lighter, thinner and better; but this has led to a

sacrifice in the space-size of a device and due to this lack of space it is harder to improve this technology [52]. Contraction of space-size has reduced the space allotment for storage unit such as batteries which has led towards less capacity of the device to store energy. These problems can be solved by developing a self-sustaining and self-charging battery using energy from the ambient environment. Since, human motion can be affiliated to the usage of the electronic devices, utilizing the mechanical motion through TENG claims to be the solution of this problem [53–61].

In order to create a TENG that does not affect the ease of use, shape and efficiency of an electronic device, investigation has to be done for selecting the most proper materials that could address these requirements [62,63]. In the first part of this work, a cost-effective energy case of unique design including two single electrode TENG was constructed to utilize the energy from the mechanical motion while using or carrying the touch electronic device and use this energy to power these smart devices. In the front part of the device a single electrode based TENG was fabricated for the front part of a cellphone without covering the screen and, at the same time, protecting it without affecting the functionality of the device, transparent materials were chosen as priority and as a second priority by their hardness and strength[64–68]. Selecting PET material as the best choice covering these requirements and looking for a new way to recycle it, it was found as the ideal material to create a TENG for the front part of the device [69]. This first TENG works with one fundamental principle proper of it, single-electrode mode [70–72]. By attaching PET on the screen of the cellphone and putting copper connected to a small surface of the material by one side of the cellphone is how this TENG is made. This TENG is activated by using human skin to touch the PET surface and harvesting the mechanical energy that is commonly applied to touch a screen of a cellphone and then transform it into electrical

energy[73–75]. The front part was further modified using Ag nanoparticles over the PET film which was tested at 120 Beat Per Minute (BPM) load frequency. The output response was compared with the obtained results from the primary device as well.

The second nanogenerator is located on the back part. We wanted to take completely advantage of the mechanical energy created by a human so we developed a TENG that can take mechanical energy by walking[76,77]. This is made with NBR and Polyethylene. The polyethylene is placed on the back part of the smart phone, NBR, and a spacer that prevents each material from continually touching each other. NBR was used for fabricating the TENG at the back part as it gave good response with PET. It works through frictions as a single-electrode TENG [60]. The motion that is created by walking is enough to make these two materials touch each other. Combining the both parts, the device can be called Triboelectricity based Stepping and Tapping Energy Case (TESTEC). TESTEC showed the potential to utilize the mechanical energy that is related to the daily life usage of smart electronic devices. The application of TESTEC into different electronics seeks to be the solution for the creation of cost effective and self-sustaining electronic devices for the near future[78].

In the seconds part of this work, we have synthesized KNN through ball milling process and incorporated the synthesized KNN into PVDF matrix along with MWCNT to fabricate a lead-free hybrid energy film (EF) for harvesting mechanical energy through triboelectric and piezoelectric mechanism. The synthesized KNN particles was characterized using X-Ray Diffraction (XRD) spectroscopy and Scanning Electron Microscopy (SEM). The film was attached with Copper electrode to convert it into a PENG and tested at variable load frequency (60, 120, 180 and 240 BPM). The output piezoelectric voltage of the device was also tested at variable pressure from 10 to 40 PSI with pneumatic piston to analyze its pressure sensitivity.

Besides, the energy film was studied at different finger motion. A hybrid piezoelectric and triboelectric nanogenerator was fabricated to test the effect of triboelectricity along piezoelectricity. Also, three different types of film with 3%, 4% and 5% KNN were synthesized and tested. Furthermore, the hybrid film was integrated with bridge rectifier, capacitor and LEDs to check its compatibility with conventional electronic components. Lastly, the energy film was attached with Kapton to utilize the high triboelectric effect of Kapton along with the piezoelectric effect of the energy film. Overall, the experiment was performed with an aim to develop a lead free triboelectric and piezoelectric composite film for efficient biomechanical energy harvesting and sensory applications with a aim for promoting sustainable future.

CHAPTER II

SYNTHESIS AND FABRICATION OF SELF-SUSTAINABLE TRIBOELECTRIC ENERGY CASE FOR POWERING SMART ELECTRONIC DEVICES

Objective

In order to create a TENG that does not affect the ease of use, shape and efficiency of an electronic device, investigation has to be done for selecting the most proper materials that could address these requirements [62,63]. In this work, a cost-effective energy case of unique design including two single electrode TENG was constructed to utilize the energy from the mechanical motion while using or carrying the touch electronic device and use this energy to power these smart devices. In the front part of the device a single electrode based TENG was fabricated for the front part of a cellphone without covering the screen and, at the same time, protecting it without affecting the functionality of the device, transparent materials were chosen as priority and as a second priority by their hardness and strength[64–68]. Selecting PET material as the best choice covering these requirements and looking for a new way to recycle it, it was found as the ideal material to create a TENG for the front part of the device [69]. This first TENG works with one fundamental principle proper of it, single-electrode mode [70–72]. By attaching PET on the screen of the cellphone and putting copper connected to a small surface of the material by

one side of the cellphone is how this TENG is made. This TENG is activated by using human skin to touch the PET surface and harvesting the mechanical energy that is commonly applied to touch a screen of a cellphone and then transform it into electrical energy[73–75]. The front part was further modified using Ag nanoparticles over the PET film which was tested at 120 Beat Per Minute (BPM) load frequency. The output response was compared with the obtained results from the primary device as well.

The second nanogenerator is located on the back part. We wanted to take completely advantage of the mechanical energy created by a human so we developed a TENG that can take mechanical energy by walking[76,77]. This is made with NBR and Polyethylene. The polyethylene is placed on the back part of the smart phone, NBR, and a spacer that prevents each material from continually touching each other. NBR was used for fabricating the TENG at the back part as it gave good response with PET. It works through frictions as a single-electrode TENG [60]. The motion that is created by walking is enough to make these two materials touch each other. Combining the both parts, the device can be called Triboelectricity based Stepping and Tapping Energy Case (TESTEC). TESTEC showed the potential to utilize the mechanical energy that is related to the daily life usage of smart electronic devices. The application of TESTEC into different electronics seeks to be the solution for the creation of cost effective and self-sustaining electronic devices for the near future[78].

Experimental Procedures

Synthesis of SETENG for Primary Testing

4cm X 3cm Cu films were used to synthesize SETENG for primary testing. Commercially available PET, PE and PP films of the same dimension were attached with the Cu films. An extension of the Cu film was added for attaching the device with alligator clips.

Polydimethylsiloxane (PDMS) based SETENG was synthesized using 2g PDMS (Sylgard 184 Silicone Elastomer Base) and 10wt% curing agent (Sylgard 184, Elastomer Curing Agent). The reagents were mixed using vortex mixer for proper mixing. Then the mixture was placed on the Cu film using Doctor's Blade technique following by drying in the room temperature for 36 hours.

Synthesis and device fabrication

The cellphone used for this experiment was a Samsung J5 and a case of the company Writeright for this phone as well. The materials used for the frontal part of the TESTEC were a commercial PET film and copper tape. The PET film was cut 8cm X 4cm leaving a small extra surface equality form to the side of it and then cleaned with ethanol. A copper tape was attached to one side of the device. Then the small extra surface previously left was bent and placed over the copper tape. The PET film was attached with tape from the exterior part.

The back part of the TESTEC was made with NBR (VWR), PET, and copper. A copper film was cut with 9cm x 6cm dimensions not bigger than the device. It was cleaned with ethanol and placed in the center on the back part properly attached with copper tape maintaining a

connection with the copper tape previously attached to one of the sides of the device. A PET film was cut with the same dimensions of the copper foil, cleaned with ethanol and attached over the copper foil with tape. The material used for the spacer is Polyurethane foam, it was cut in a 5.5 cm x 7.5 cm with a thickness of 0.3 cm and then cut from the inside leaving a 0.8 cm of width giving us a shape of frame. After that it was attached with glue over the polyethylene film. The NBR film followed the same process cut with similar dimensions as the other materials, cleaned with ethanol and attached with copper tape.

The TESTEC was further modified using Ag nanoparticles on the PET film. Ag nanoparticles were sputtered on the PET film using a magnetron sputtering system (AJA International inc: ATC- Orion-5UHV) at rate of 0.5nm/sec (10nm thick). The modified PET film was then attached with the case like the previous steps discussed.

FTIR Characterization:

The Fourier Transform Infrared Spectra of the PET and NBR film were obtained using VERTEX 70v FTIR Spectrometer (Bruker) in Attenuated Total Reflection (ATR) mode. Transmittance of the both samples were recorded at wavelength from 450cm^{-1} to 4000cm^{-1}.

UV-Vis Characterization:

The UV-Vis spectra of the modified PET film were performed using Perkin Elmer Lambda 950 UV-Vis Spectrometer from 250cm^{-1} to 800cm^{-1}.

Measuring of Output:

The output voltage signal from the TESTEC was characterized with Tektronix TDS1001B digital oscilloscope, while the current signal was measured using low noise current pre amplifier (Stanford Research SR570). For further confirmation VersaSTAT 3 potentiostat and Tektronix A622 current probe were used for voltage and current measurement respectively. The entire test was carried out in ambient environment.

Results and Discuission

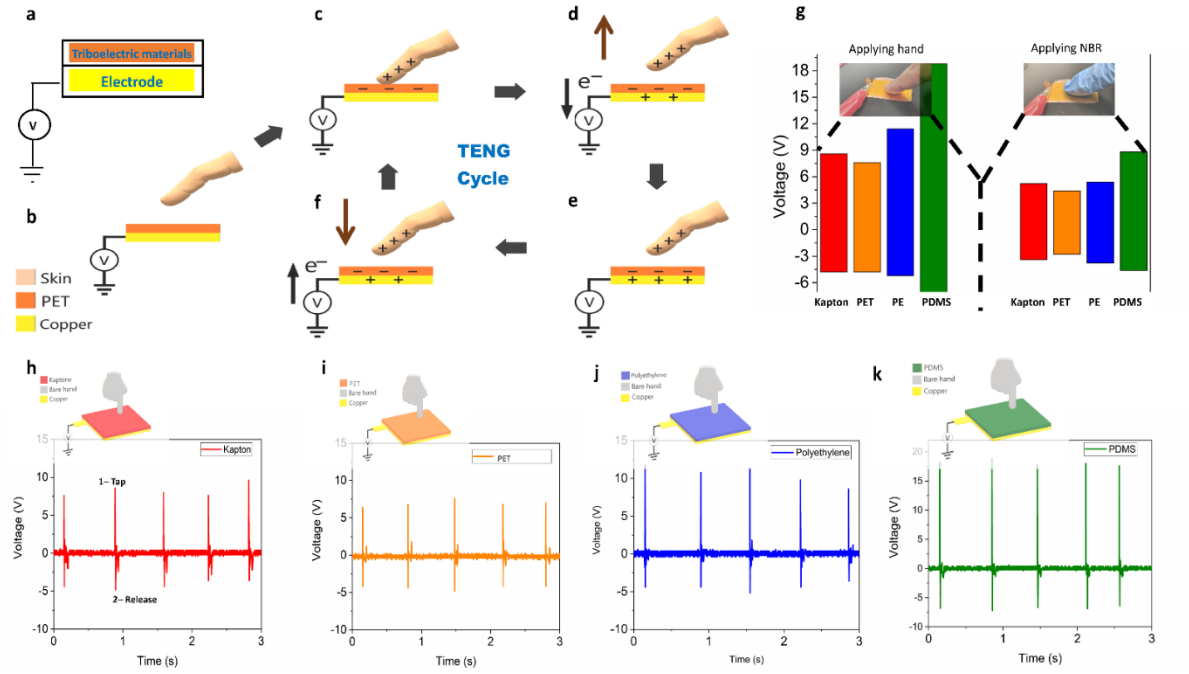

Figure 1: (a) Single Electrode Triboelectric Nanogenerator for primary testing. Working Mechanism: (b) Initial stage of the TENG, (c) Full contact with the finger, (d) Finger released from the TENG, (e) Full separation from the TENG, (f) Finger moving towards the TENG, (g) Maximum peak to peak voltage observed applying hand and NBR for different materials. Voltage observed applying hand with (h) Kapton, (i) PET, (j) Polyethylene (PE), and (k) Polydimethylsiloxane (PDMS).

Testing the triboelectric output for finger tapping with different materials

Finger 1a shows a single electrode triboelectric nanogenerator (SETENG) which was fabricated to test the triboelectric effect due to finger tapping motion with different materials and select proper material for the energy case. The testing device was basically consisted of a layer

of testing material and a Copper electrode. The test was run by applying tapping motion on the device with bare fingers and NBR covered fingers. Human skin and NBR has low affinity for surface electron according to the triboelectric series [60,79]. To obtain higher triboelectric effect with finger and NBR , the testing materials were selected considering their lower position in the triboelectric series[80]. Hence, Kapton (Polyimide), Polyethylene tetraphthalate (PET), Polyethylene(PE) and Polydimethylsiloxane(PDMS) were used as the materials for primary testing due to the position in the triboelectric series [79,81–83].

The working principle of the single electrode triboelectric nanogenerator using tapping motion between finger and PET was explained through figure 1b to 1f. The mechanism can be explained as a combination of contact triboelectrification and electrostatic induction [4,84] Figure 1b shows the initial position of the finger which is kept at a certain distance from the SETENG. When tapping operation is started the finger gets in contact with the PET layer (Figure 1c). Due to the higher surface charge affinity of PET electron transfers from the skin to the PET layer resulting contact triboelectrification between these two surfaces [4,60,79,83,85,86]. As the finger starts separating from the PET layer, electrons start moving to the ground from the Cu electrode to compensate the effect of contact triboelectrification of the PET surface (Figure 1d). An output voltage signal can be observed at the output due to this effect of electrostatic induction. Eventually, the electron stops flowing after the complete separation of these two layers as the electrons of the PET surface gets balanced by the induced positive charges of the electrode (Figure 1e). No output voltage can be observed at this stage. The finger starts moving towards the PET layer again (Figure 1f). As the positive charges on the finger gets closer to the PET surface, the electrons start moving to the electron to maintain the charge balance resulting a reversed output voltage. This cycle continues until the tapping motion is stopped. This

mechanism is applicable for Kapton, PE and PDMS as well. The intensity of the output signal highly depends on the materials. Besides, the output also depends on variable parameters like distance of impact, tapping frequency, contact area etc.

The primary testing was performed at 90 BPM (1.5Hz) tapping frequency keeping 3 cm as the distance between the index finger and the testing materials. The results showed different reading of open circuit voltage for different testing materials. Figure 1g demonstrates the maximum peak to peak voltage obtained from the SETENG for tapping motion with bare and gloved index finger on Kapton, PET, PE and PDMS film. Besides, figure 1h-k demonstrates the output voltage signal for tapping kapton, PET, PE and PDMS respectively with bare fingers for 3s time interval. With the application of stress with finger the output voltage rises to the maximum point 1(Figure 1h). However, the direction of the electron flow changes with the release of pressure resulting reversed output voltage which reaches up to point 2 (Figure 1h). Point 1 and point 2 can be defined as the maximum and the minimum peaks of voltage. It is clear from the figures that the PDMS film showed highest triboelectric output by interacting with the bare finger compared to the other materials. The PDMS-finger interaction generated a highest voltage of 18.8V and a peak to peak voltage of 7.2V (Fig 1g and 1k). However, kapton, PET and PE also showed decent response with the finger which generated highest output voltage of 8.6 V (Fig 1h), 7.6 V (Fig 1i) and 11.5V (Fig 1j) and peak to peak voltage of 13.4 V, 12.4 V and 16.7 V (Fig 1g), respectively. According to the triboelectric series the PDMS has the higher electron affinity compared to kapton, PET or PE [81]. This higher affinity of electron leads towards higher triboelectric output due to the interaction with bare fingers. On the other hand, it was also observed that tapping motion with bare fingers produced compared to the fingers with NBR gloves (Fig 1g). The maximum open circuit voltage and peak to to peak voltage using the NBR-

PDMS interaction was observed to be 8.8V and 13.4V respectively. Besides, the maximum peak to peak voltage for kapton, PET and PE was measured to be 8.6V, 7.3V and 9.2V respectively. The NBR has lower position compared to the human skin according to the triboelectric series. It has a charge affinity of +3nC/J which is quite low compared to the charge affinity of human skin(+30nC/J) [79]. Hence, it exhibits lower triboelectric effect than the human skin. The results of the primary testing clearly shows the prospect of using finger taping to generate electricity with kapton, PET, PE and PDMS.

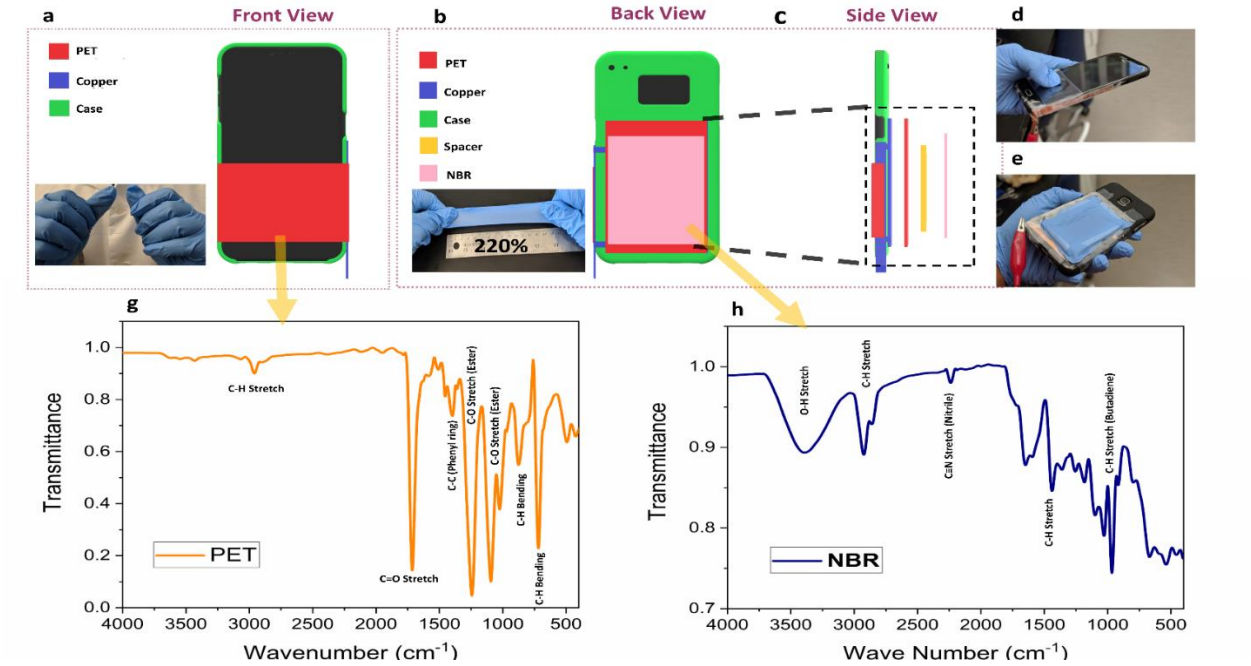

Figure 2: (a) Front view (inset: transparent PET films), (b) Back view (inset: Highly stretchable NBR films), and (c) Side view of the mobile attached TESTEC schematic. (d) Front part an, (e) back part of the optical view of the TESTGC. Fourier-transform infrared spectroscopy (FTIR) spectra of (f) PET film and (g) NBR film.

Triboelectricity based Stepping and Tapping Energy Case (TESTEC): Materials and Characterization

Touch electronic devices has become an integral part of everyday life of a big portion of World's population. According to Dscout research firm, a touch phone is on average being touched about 2617 times by a person everyday [87]. To utilize the mechanical energy from touching motion a Triboelectricity based Stepping and Tapping Energy Case (TESTEC) was built based on the results of the primary testing discussed in the previous section. The front part of the TESTEC consists of a rectangular shape transparent PET film and a Copper electrode which attached with the PET film (Fig 2a). PET showed good triboelectric response during the interaction with hand and NBR discussed in the previous section. These cost effective thermoplastic have been widely used as touch screen protector due to its high strength, transparency and light weight as well as resistance to impact, shatter and scratch [88–90]. On the other hand, the back part includes a PET and NBR film separated by air gap with the help of a rectangular shaped spacer foam. A Copper film is attached with the PET film which works as an electrode. Figure 2b and 2c demonstrates the back and side view of the TESTEC respectively. NBR is a highly flexible and cost effective polymer [91,92]. It showed good triboelectric response while examining interaction between PET film and NBR gloves mentioned in the previous section. The front and back part of the TESTEC was designed to utilize mechanical energy directly from finger tapping and indirectly from foot stepping.

The characterization of the PET and NBR film was performed through Fourier Transformation Infrared (FTIR) Spectroscopy using Attenuated Total Reflection (ATR) technique. Figure 2d provides graphical demonstration of FTIR spectra of the PET film from 400 to 4000 cm^{-1}. The asymmetric sharp peak at 1095 cm^{-1} and the symmetric sharp peak at 1243 cm^{-}

^{1} are due to the C-O stretch of Este. Besides, the peak at 1394 cm^{-1} comes from the vibration of C-C from the phenyl ring. Also, the sharp peak at 719 cm^{-1} denotes C-H bending from the out of plane benzene group. Furthermore, the C=O stretch resulted a sharp peak at the wavelength of 1714 cm^{-1} [93–96]. On the other hand, figure 2e shows the FTIR spectra of the NBR film. The peak at 2237 cm^{-1} confirms the presence of nitrile group (C≡N). Also, the peak at 966 cm^{-1} corresponds the C-H stretch from Butadiene group. Besides, the peaks at 1440 cm^{-1} and 2923 cm^{-1} attributes to the C-H stretch of NBR rubber [97,98].

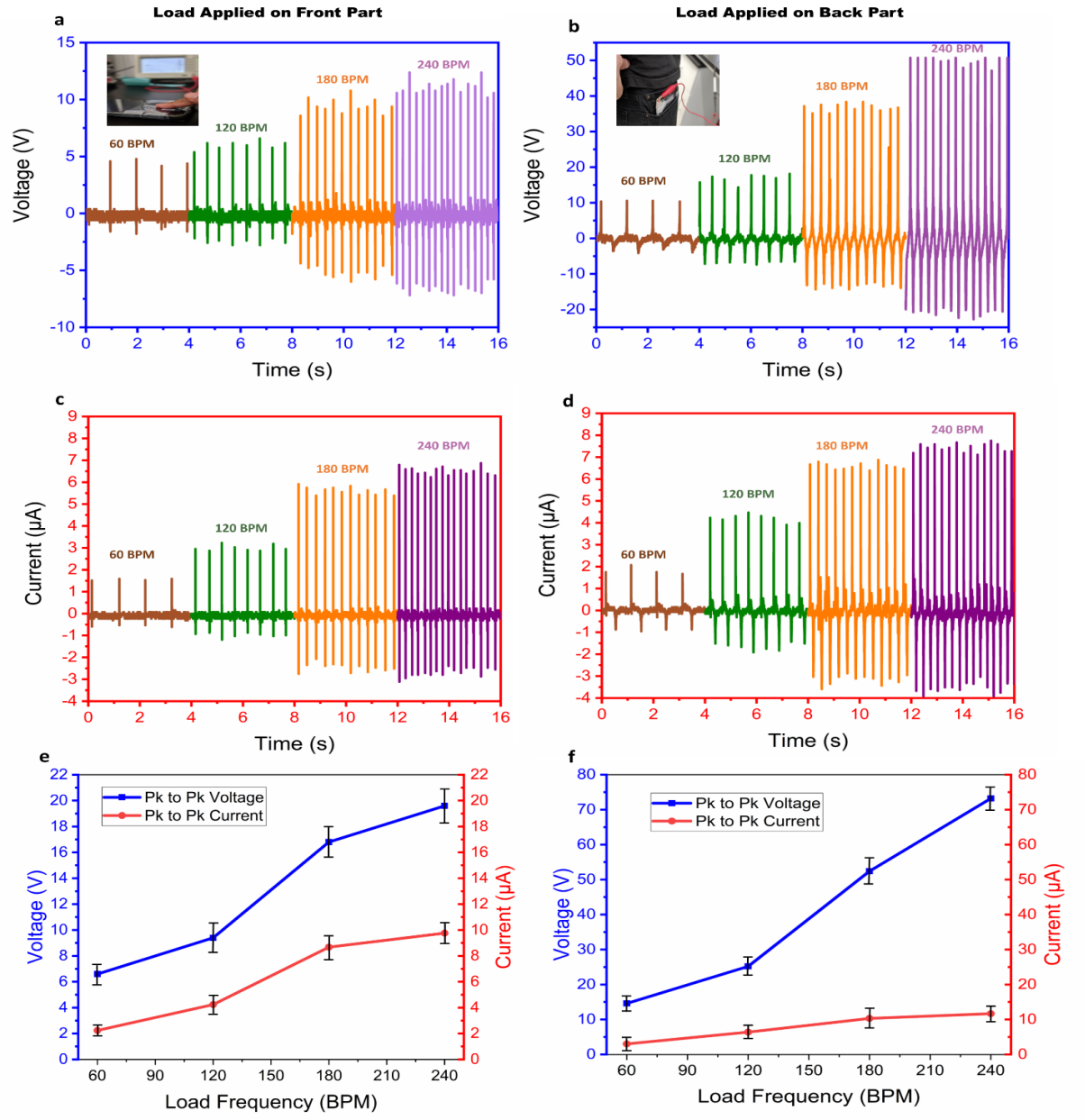

Figure 3: Voltage observed for different load frequency on (a) front part (inset: Device during tapping on the front part) and (b) back part (inset: Device during stepping). Current observed for different load frequency on (c) front part and (d) Back part. Comparison of maximum peak to peak voltage and current observed for (e) front part and (f) back part with error bars (Standard deviation for 3 readings)

Output performance of TESTEC under variable frequency, air gap and fingertip combinations

The output characterization of TESTEC was performed under variable load frequency. The front part of the device was tapped with the index finger at 60 BPM (1Hz), 120 BPM (2Hz), 180 BPM (3Hz) and 180 BPM (4Hz) frequencies keeping 3cm surface gap (Fig 3a inset). Also, the back part was tested by stepping at the same frequencies maintaining 5cm surface gap between the shoe sole and the floor while the device was set at the pocket (Fig 3b inset). The supplementary movie 1 and 2 demonstrates the tapping and stepping test of the TESTEC at 120 BPM. The stepping motion results in movement of the thigh which vertically pushes the back part of the TESTEC and creating triboelectric effect. Figure 3a and 3b shows the open circuit voltage at output recorded at variable load frequency for the front and the back part of the TESTEC respectively. On the other hand, Figure 3c and 3d demonstrated the short circuit current at output for the same load condition. The maximum output voltage observed for the front part was 4.8, 6.6, 10.7 and 12.4 V (Fig 3a) for 60, 120, 180 and 240 BPM load frequencies respectively. Besides, the corresponding maximum output currents were 1.6, 3.2, 5.9 and 6.9 µA (fig 3b). The impact velocity increases parallelly with load frequency. As a result, the electrons in the external circuit gets shorter time to neutralize the triboelectric potential leading towards a larger flow of electron [4,99–101]. Hence, the increment in the frequency leads towards larger current. Correspondingly, the output voltage increased with the increase of current as voltage is a linear function of the current [100,101]. However, the back part showed higher output response due to the stepping motion. The maximum output voltage for the back part were recorded as 10.6, 17.8, 38.4 and 50.8V whereas the currents were 2.08, 4.48, 6.88 and 7.76µA respectively. PET showed higher response with human skin compared to the NBR in the primary experiment

discussed above. However, the back part of the device involved higher surface area(54cm^2) in the triboelectric action between the NBR and PET The finger tapping on the front part only involved the surface area about 6.67cm^2 (index finger tip volar) [102]. The higher surface area resulted higher charge transfer between the surfaces leading towards higher triboelectric output of the back part [103,104]. But the front part showed higher output based on current density. Compared to the maximum current density of 0.14 μA/cm^2 of the back part at 240 BPM, the front part exhibited a maximum current density of 1.03 μA/cm^2. Figure 3e and 3f demonstrates a graphical representation of maximum peak to peak output voltage and current observed at variable load frequency for the front and back part respectively. The peak to peak current and voltage increased linearly for both parts with increasing frequency. However, the rate of this increase is lower for the peak to peak current of the back part which is promoted due to the higher resistivity of NBR compared to human skin [105,106].

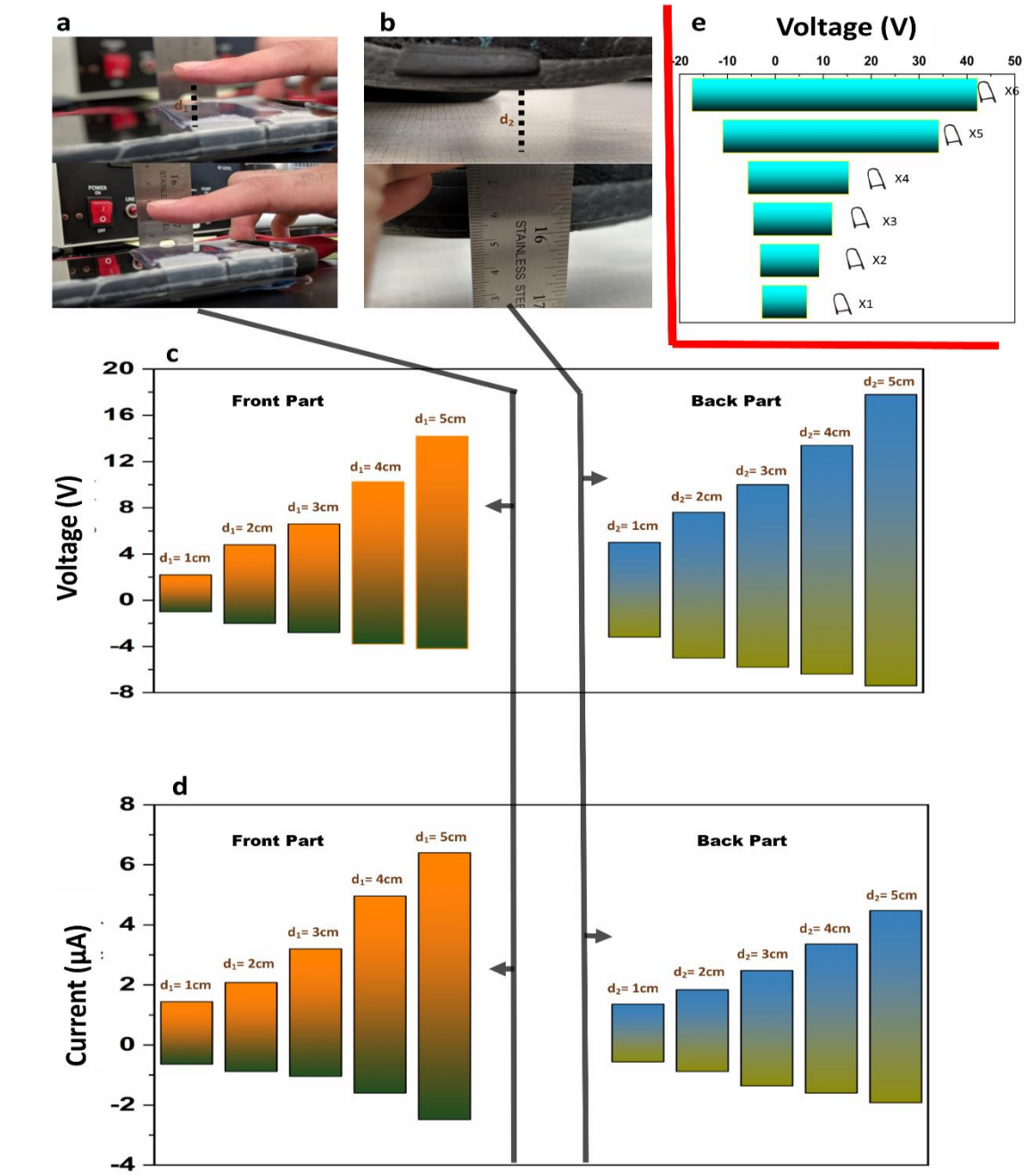

Figure 4: (a) Tapping and (b) Stepping Test at variable distance. (c) Observed voltage at variable distance for the front and back part. (d) Observed current at variable distance for the front and back part. (e) Observed maximum voltage at variable fingertip combination

The output performance of the TESTEC was also tested for variable air gap between the operating surfaces. The test was performed at 120 BPM tapping and stepping frequency with a variable airgap from 1 to 5 cm for the front (Figure 4a) and back (Figure 4b) part respectively. As the airgap increased from 1cm to 5 cm, the voltage increased linearly from 2.2 to 14.2 V for the impact on the front side as well as from 5 to 17.8 V for the impact on the back side (Figure 4c). As the airgap increases, the force due to the impact on the triboelectric surface also increases directly for the front side and indirectly for the back side. Since the frequency of tapping is kept constant, the velocity of the finger increases with increased airgap. So, the momentum increases with the increased velocity concluding towards higher force of impact. This magnified force leads to larger deformation of the contact surface of the triboelectric layers resulting higher surface area and higher output voltage [100,107,108]. The output current also increased linearly with increasing airgap. While the maximum output current was observed as 1.5 μA for the front part at 1cm airgap, the output current increased to 6.4 μA at 5 cm airgap. Likewise, The output current increased from 1.3 to 4.5 μA for the back part. As discussed before, the velocity of the finger increases due to the increased airgap with constant frequency of impact. So, The kinetic energy on the triboelectric layer increases with the increase of velocity which leads towards larger transfer of electrons through the triboelectric surfaces [100,107]. As a result, electrons from the electrodes flow at a higher rate to neutralize the larger transfer of electrons of the triboelectric surfaces which results higher output current in the output.

The output performance of TESTEC was further tested by tapping with multiple fingers. The front part of the device was tapped at 3 cm airgap and 120 BPM frequency using different combination of fingertip. The volar section of the index, middle and ring fingers of both hands were used for this test. Figure 4e demonstrates maximum peak to peak voltage obtained for

variable fingertip combination at the output. The maximum peak to peak voltage using the index fingertip was 9.4 V. As the middle finger was added with the index finger the peak to peak voltage increased to 12.3 V. The surface area of the contact triboelectrification increased from 6.67 cm^2 to 13.84 cm^2 when the middle fingertip was added with the index finger [102]. The higher surface area of the combined index and middle fingertip promoted higher triboelectric output [104,109]. The highest peak to peak voltage was obtained for the combination of index, middle and ring fingertip of both hands (59.6 V). However, the output signal did not rise linearly due to the unequal surface area as well as variation of impact of the fingers. When the index finger of the left hand was added with the other three fingers (index, middle and ring fingers) of the right hand, the output signal increased exponentially as the index finger of the left hand created higher impact combining with the other three fingers of the right hand.

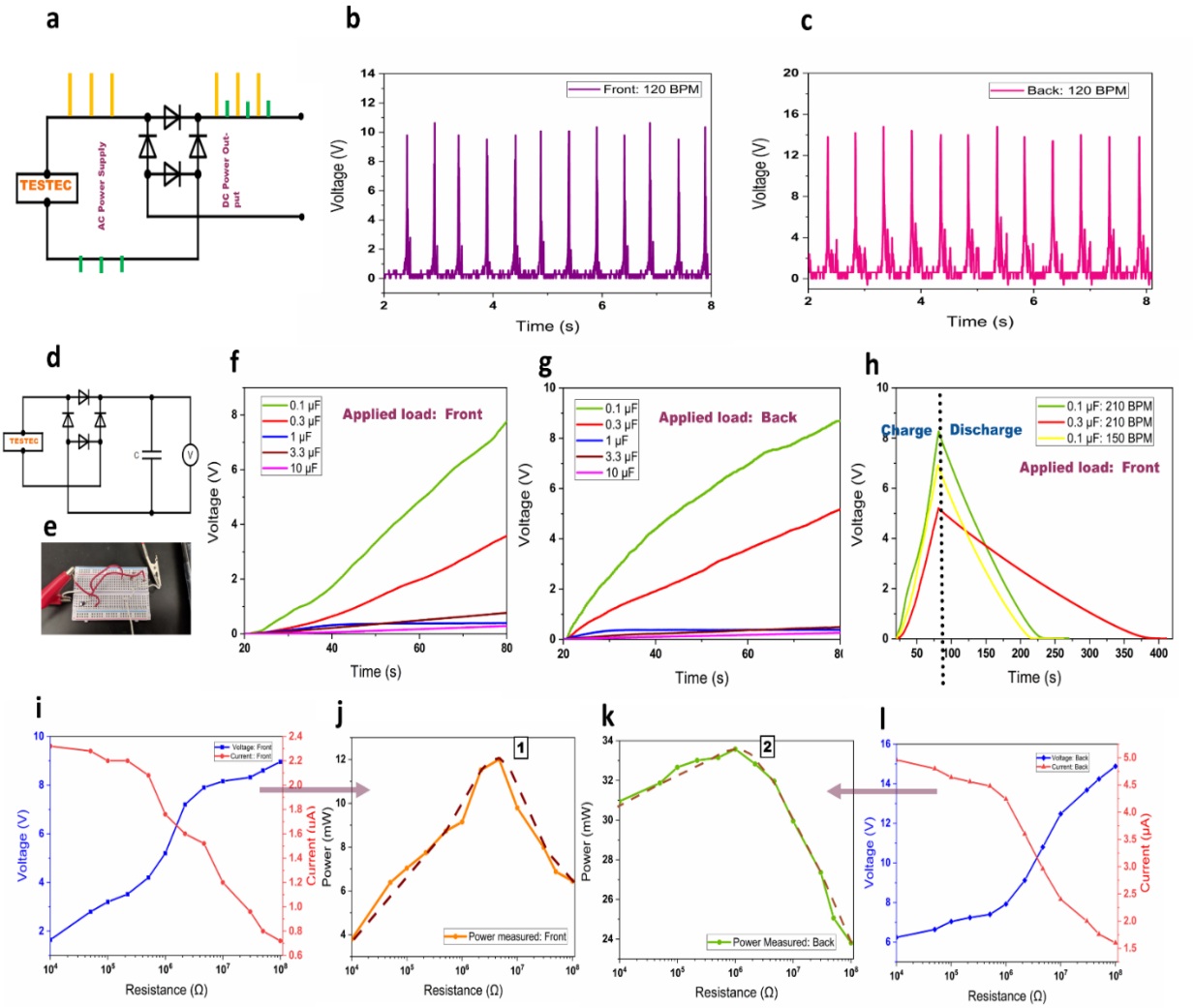

Figure 5: (a) Circuit diagram for rectifying the signals by TESTEC. Rectified voltage signal at 120 BPM load frequency for (b) front part and (c) back part. (d) Schematic circuit diagram and (e) Optical view of circuit diagram for charging and discharging capacitors with TESTEC. Charging capacitors of variable capacitance for 60 seconds by applying load on the (f) front part and (g) the back part of the TESTEC. (h) Ability of the TESTEC to charge and capacitors for different load frequencies by applying load on the front part. (i) Average voltage and current measured at variable external resistance with front part of the TESTEC. (j) Average power measured by applying load on the front part of the TESTEC at different external resistances. (k)

Power measured by applying load on the front part of the TESTEC at different external resistances. (l) Average power measured by applying load on the back part of the TESTEC at different external resistance.

Integration of The TESTEC with conventional electronic components

The output performance of the TESTEC was also tested with conventional electronic components. Firstly, the output response of TESTEC was studied by integrating with a full wave bridge rectifier. Figure 5a demonstrates the equivalent circuit diagram for converting the AC power signal to DC signal. Figure 5b and 5c shows the full wave rectified voltage signal obtained from tapping the front and back part of the device at 120BPM frequency and 5cm airgap respectively. The maximum output rectified open circuit voltage was recorded as 10.6 and 14.8V for the front and back part respectively. Point 1 and 2 from figure 5b shows the rectified output signal due to tapping and releasing on the front part respectively while the point 3 and 4 from figure 5c shows it for step down (press) and step up (release) motion operating the back part. The output signal from releasing operation is quicker for the front part compared to the back part as the direct contact and release of the front part results quicker separation between contact surfaces compared to the indirect contact and release of the back part.

After examining the device with the full bridge rectifier, the device was examined with capacitor to test the prospect of storing energy from the tapping and stepping motion as well as providing constant bias voltage to power touch based electronic equipment [107,110]. Figure 5d and 5e demonstrates schematic and optical view of the equivalent circuit diagram where the device was integrated with a full bridge rectifier and a capacitor. Capacitors of 0.1, 0.3, 1, 3.3 and 10 μF were used for the test at 5cm airgap. Figure 5f and 5g shows the open circuit voltage for charging the capacitors for 60 seconds at 210 BPM frequency using the front and back part of

the TESTEC respectively. The higher the capacitance of the capacitor, the lower the rate of charging. For instance, the output voltage observed for 0.1 µF was 7.7 V which was 3.6 V for 0.3 µF capacitor after charging it for 60 s using the front part. Similarly, the discharge rate was higher for the 0.1 µF capacitor. It took 145 s for discharging the 0.1 µF capacitor completely where it took 302 s for the 0.3 µF capacitor (Figure 5h). In case of the back part, the output voltage with the capacitors of 0.1 and 0.3 µF was measured as 8.7 and 5.2 V respectively. The 0.3 µF capacitor charges slower than the 0.1 µF capacitor due to the higher loss of charges in the capacitor [107,110,111]. In addition, the output voltage of the front part with the 1, 3.3 and 10 µF capacitors were observed to be 0.78, 0.4 and 0.29 V respectively after charging the capacitors for 60s. Likewise, this output voltage was 0.38, 0.49 and 0.25 V for the back part. Furthermore, the effect of variable frequency was observed for charging and discharging the 0.1 µF capacitor with the front part of the TESTEC (Figure 5h). The rate of charging at 210 BPM was higher than 150 BPM. As the number of contacts is larger in case of 210 BPM frequency, larger number of charges transfer from the finger to the PET film during charging operation. Hence, higher output voltage can be obtained which results higher rate of charging. However, the rate was observed to be lower for 210 BPM in case of discharging. Due to the accumulation of higher voltage during charging operation, it takes more time for discharging the capacitor at 210 BPM tapping frequency. The energy conversion efficiency was measured based on the output energy from the capacitor test. The input energy was ideally considered to be the initial potential energy from the finger and the foot in 5cm height. The maximum energy conversion for 0.3µF capacitor was calculated to be 57.4% for the front part and 4.46% for the back part. The direct impact on the PET layer from the finger resulted in higher efficiency of the front part of the device. On the

other hand, the back part was driven indirectly by the contact between the foot and the floor which resulted intermediate loss of energy and lower energy conversion efficiency.

The output power, voltage and current of the TESTEC were also characterized with external loads from 10^4 to 10^8 Ω for both parts. With the increase of the resistance the output voltage rises while the output current decreases following the Ohm's law (Fig 5i and 5l). Nevertheless, a sharper increment of the voltage can be observed from 0.25 and 0.5 MΩ resistance for front and back part correspondingly. This inverse tends of the output voltage and current leads towards the measurement of power at optimum resistance. Figure 5j and 5k shows Power measured for the front part and the back part respectively. The corresponding maximum power obtained from the TESTEC was 12.1 mW (3.78 mW/m^2) at 0.46 MΩ for the front part and 33.56 mW (6.21 mW/m^2) at 1.02 MΩ for the back part.

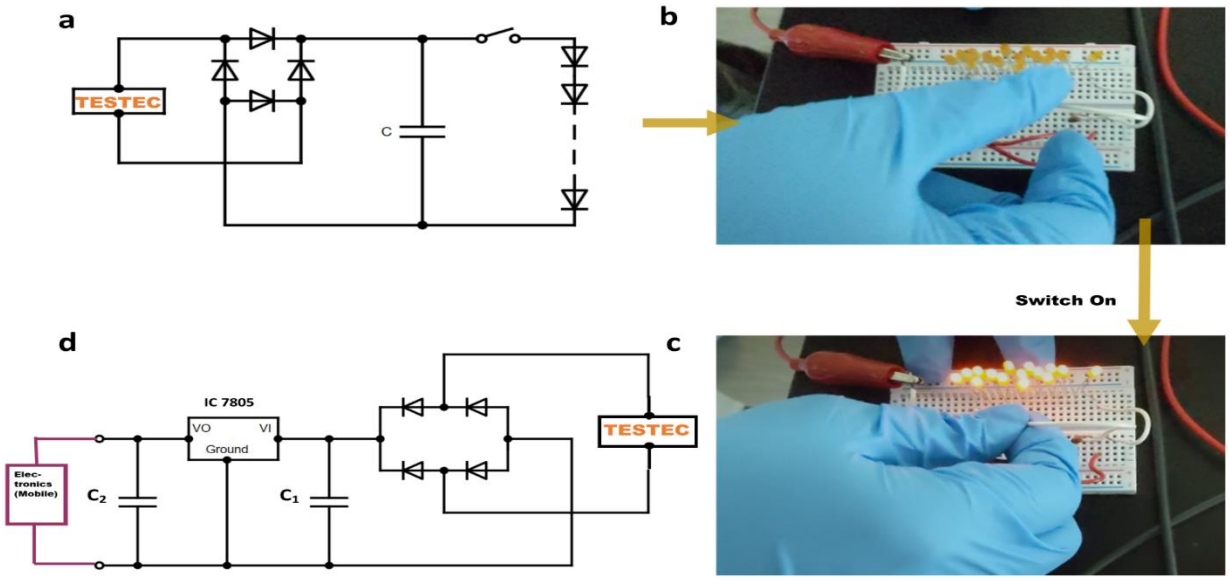

Figure 6: (a) Circuit diagram for powering LED's with TESTEC. (b) Switch off mode of the circuit. (c) Lighting 15 LEDs with the TESTEC. (d) Proposed Circuit diagram for charging electronics (mobile phone).

Powering smart electronics with TESTEC

In the previous sections, energy harvesting and storing capability of the TESTEC has been discussed at different conditions. For further application, we investigated the TESTEC for lighting commercial Light Emitting Diodes (LED). Figure 6a shows equivalent circuit diagram for lighting commercial LEDs with TESTEC. A series of LEDs were attached with a capacitor and a full bridge rectifier. The front part of the TESTEC was switched off and tapped at 120 BPM frequency for 60 seconds (Figure 6b). After switching on the circuit, 15 commercial LEDs were lightened with the TESTEC (Figure 6c). The output of the LED test as well as the capacitor test magnify the prospect of the TESTEC for the application of powering smart electronic devices [24,61,86]. For instance, Most of the smart phone now a days are run by Li-ion batteries which usually operates between 1.5 to 4.2 V [112,113]. The tapping and stepping motion can be applied to partially charge these batteries. An equivalent simple circuit diagram is proposed at figure 6d to charge smart electronics with TESTEC. An IC 7805 can be used for regulating the voltage at 5 V [114]. Two capacitor C1 and C2 are used to remove AC ripples and maintain proper voltage supply at the output. Utilizing the tapping and stepping motion through TESTEC will reduce energy loss thus promoting sustainability.

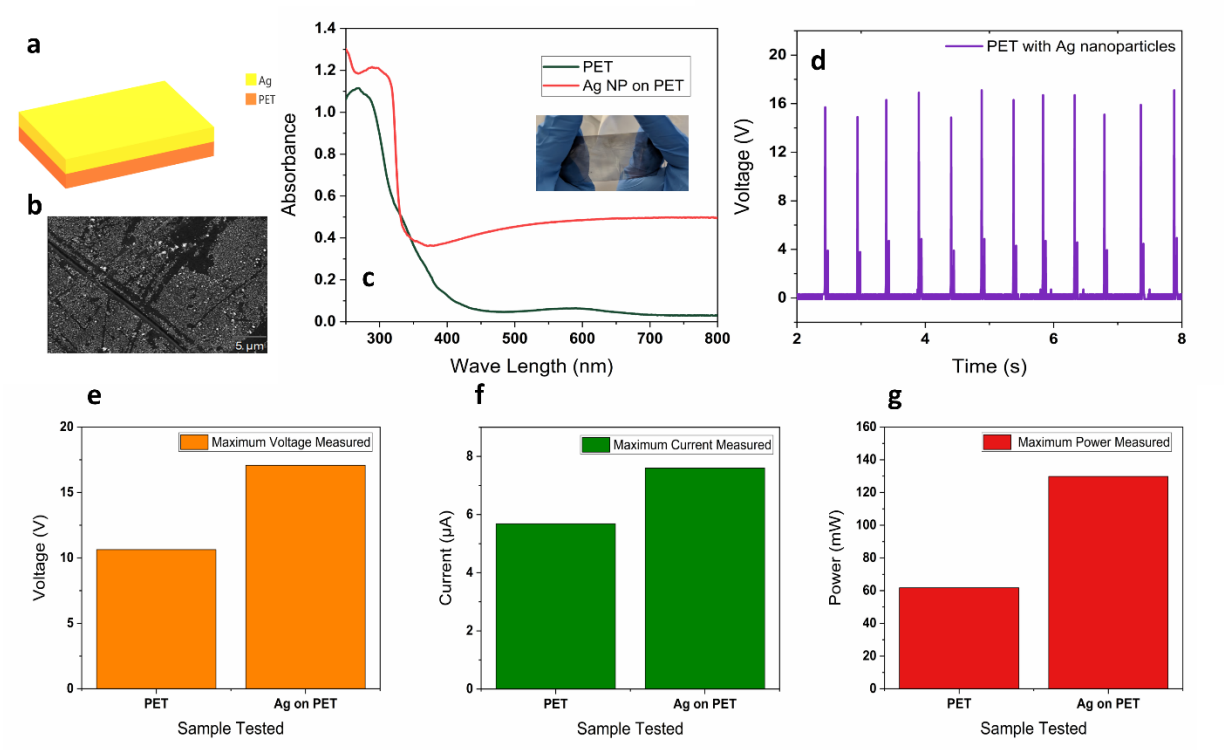

Figure 7: (a) Ag nanoparticles over PET film. (b) SEM image of Ag sputtered PET film for the modified TESTEC. (c) Ultraviolet–visible (UV) Vis Spectra of PET film with and without Ag nanoparticles. (inset: Optical view of the Ag sputtered PET fim) (d) Rectified voltage signal by the modified TESTEC at 120 BPM load frequency. (e) Comparison between maximum rectified voltages obtained from standard and modified TESTEC. (f) Comparison between maximum rectified current obtained from standard and modified TESTEC. (g) Comparison between maximum rectified power obtained from standard and modified TESTEC.

Modification of TESTEC: Application of Ag Nanoparticle

To obtain performance from the TESTEC Ag nanoparticle were used on the PET film. A very thin layer(10nm) of Ag nanoparticles were sputtered on the PET film (Figure 7a). Application of Ag nanoparticles leads to higher contact surface in triboelectric operation compared to the plain surface [115]. Although Ag nanoparticles slightly effects the transparency of the PET layer, PET layer works as a base which holed the Ag layer. Besides, the mechanical properties of the PET can be sustained during the operation of TESTEC. Figure 7b shows the SEM image of the PET layer sputtered with Ag nanoparticles. The image provides a clear view of Ag nanoparticles on the PET film. The UV-Vis spectra was used for characterizing the optical properties of the Ag/PET film [116]. Figure 7c shows the UV-Vis spectra of Ag particle-deposited PET film and commercial PET film. The maximum absorbance of the commercial PET film was observed at 266nm wavelength. However, the spectra deviated with higher absorbance for the Ag based PET film due to the presence of Ag nanoparticles[116–118]. The inset of figure 7c shows the optical view of the PET film, sputtered with Ag nanoparticles for the modified TESTEC.

The modified PET film was attached with the TESTEC for examining its triboelectric response and compared with the measured values of the plain PET surface as well. The modified TESTEC was tapped at 120 BPM with an airgap of 5cm. The results showed a higher triboelectric response due to the application of Ag nanoparticles. The maximum rectified voltage was observed to be 17.1 V (Figure 7d) which on the other hand was 10.6 V for the plain PET surface (Figure 7e). Also, the maximum output current and power were increased by 2 μA and 68.1 mW for the modified TESTEC, respectively (Figure 7f and 7g). This enhanced surface area of the modified TESTEC resulted higher output response due to the higher charge transfer in the

surface. But, this enhancement was depleted as the triboelectric response was basically observed due to the interaction between Ag and skin which has less gap in triboelectric series compared PET and skin [79,83]. Modification of the TESTEC showed the prospect of scavenging more energy compared to the standard TESTEC.

Conclusion

In summary, we have designed a cost effective and adjustable energy case (TESTEC) with commercial PET and NBR films to harvest mechanical energy through triboelectric mechanism. It was designed to adjust with touch electronic devices and power them directly from tapping and stepping motion while using and carrying the electronic devices. The TESTEC successfully converted mechanical energy into electrical energy in which the output response by the device was increased linearly with increased frequency and airgap during tapping and stepping operation. The maximum output voltages of the front and back parts were measured as 14.8 and 50.8 V, respectively. Also, the output voltage raised up to 59.1 V when the front part was tapped with 6 fingers altogether. Further development of the TESTEC can be conducted for increasing the output current. In addition, the TESTEC showed an excellent response when it was integrated with capacitors, resistors and bridge. Also, it was successfully applied for charging capacitors and driving commercial LEDs rectifier which amplifies its prospect in utilizing mechanical energy through electrical energy. Furthermore, the modification of the TESTEC with Ag nanoparticles resulted higher output response. The output power was increased by 68.1 mW due to the application of Ag nanoparticles on the TESTEC. In future, the TESTEC can be tested with other nanoparticles like Au, Si and Cu as well for further development. Besides, the front part can be investigated with materials like polyurethane, tempered glass and Polypropylene for better outputs. This device holds a lot of potential for utilizing recyclable plastics from the environment. It has the potential to reduce the necessity of charging smart electronic devices through usual procedures. Promoting the TESTEC in industrial level will also promote renewable energy and sustainable development.

CHAPTER III

KNN BASED PIEZOELECTRIC/TRIBOELECTRIC LEAD-FREE HYBRID ENERGY FILMS FOR ENERGY HARVESTING AND SENSORY APPLICATION

Objective

In this work, a Potassium Sodium Niobate (KNN) nanocube based energy film (EF) has been developed for utilizing mechanical Energy through triboelectric and piezoelectric mechanism. The KNN particles were synthesized using wet ball milling technique incorporated into Polyvinylidene Difluoride (PVDF) matrix and along with Multi Wall Carbon Nanotube (MWCNT). The film was used to develop a Piezoelectric Nanogenerator (PENG) with Copper electrodes. The piezoelectric output of the film was further tested with Copper electrodes at variable tapping frequency (60 BPM to 240 BPM) and Pressure (10 PSI to 40 PSI). The open circuit voltage increased with the increase of both tapping frequency and pressure. The maximum piezoelectric output voltage was observed to be 35.3 V while the maximum current was noted as 15.8 μA. The films also showed unique output signals for different types of finger motions. The film was further utilized to build a Piezo-triboelectric hybrid nanogenerator to check its hybrid performance. The maximum output was observed to be 54.1 V and 29.4 μA in

this case. This film was integrated with conventional electronic component (bridge rectifiers, resistors and capacitors) and tested its ability to harvest energy. The hybrid nanogenerator can charge a 0.1μF capacitor to 9.4 V in 60s. Besides, the optimum output power for the device was measured as 0.164 W. The film was further attached with a Kapton film and showed a hybrid output of 113.2 V. This experiment endorsed the potential of the KNN based energy film for multifunctional application like force, pressure and motion sensing as well as lead free energy harvesting.

Experimental Method

KNN nanocube synthesis

Potassium carbonate (K_2CO_3) (Sigma Aldrich), sodium carbonate (Na_2CO_3) (Sigma Aldrich) and niobium pentoxide (Nb_2O_5) (Sigma Aldrich) were taken based on stoichiometric calculation of the following reaction:

$$K_2CO_3 + Na_2CO_3 + 2Nb_2O_5 \longrightarrow 4(K_{0.5}Na_{0.5})NbO_3 + 2CO_2$$

Before starting the process, the carbonates were dried at 200^oC for 2h for their hygroscopic nature. Wet ball milling was performed with ethanol as a solvent and stainless-steel balls with a diameter of 0.25in at 1000RPM in a vortex mixture for 12h in a sealed round bottom Pyrex glass. After the milling, the mixture was dried at 120^0C for 24h. Then the dried materials were calcined at 900^0C for 6h to obtain the KNN nanocubes.

Preparation of the KNN/PVDF/MWCNT composite film

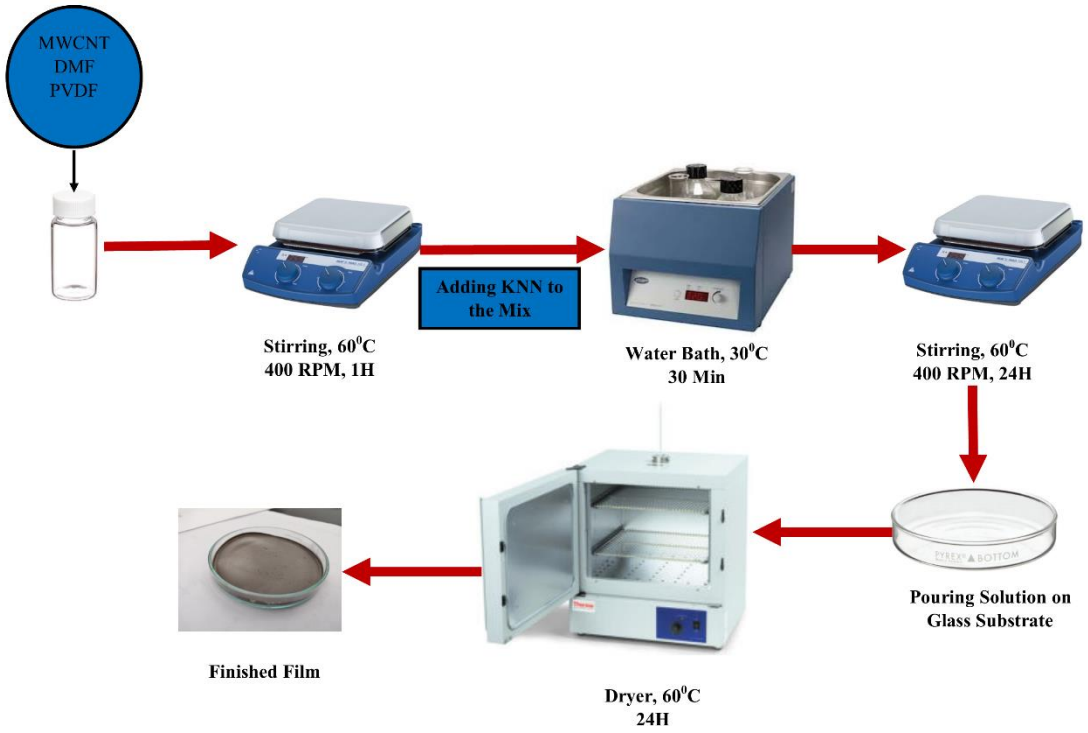

Figure 8: Fabrication process of the Film

PVDF pellets (Sigma Aldrich) and Multi Walled Carbon Nanotubes (MWCNT) were added in N, N-Dimethylformamide (DMF) (Sigma Aldrich) and the solution was stirred at 60^{0}C at 400RPM for 1h. Then the synthesized KNN nanocubes were added to the DMF solution and the solution was placed in the water bath for 30 min at 30^{0}C. After that, the solution was

continuously stirred for 24h at 400RPM and 60^0C. The mixture was then cast on the Cu electrode film and dried for 24h at 60^0C to generate the KNN/PVDF/MWCNT composite film.

Preparation of the piezoelectric and piezoelectric-triboelectric hybrid nanogenerator (PTENG)

Copper tape was added on the other side of the synthesized KNN/PVDF/MWCNT composite film to create a piezoelectric nanogenerator. The poling of the piezoelectric film was conducted at 80^0C for 2h. To create the piezoelectric-triboelectric hybrid nanogenerator (PTENG), polyurethane (PU) spacers were added between the copper tape and the top part of the synthesized composite film. This created an airgap which enabled triboelectric action to take place parallel to the piezoelectric action. A 2 in^2 polylactic acid (PLA) layer was attached to the outer side of both electrodes to impart rigidity.

FTIR Characterization

The Fourier Transform Infrared Spectra of the PVDF film, KNN nanocubes, and the KNN/PVDF/MWCNT composite film were conducted using the VERTEX 70v FTIR Spectrometer (Bruker). 450cm^{-1} to 4500cm^{-1} was the range at which the transmittance was recorded for each sample. The resolution for the analysis was 4s^{-1}.

XRD characterization

The XRD of the KNN was performed using the Rigaku Miniflex X-ray diffractometer. The output data was collected in the 2Θ range of 20^0 to 60^0 with a scanning step size of 0.015^0.

SEM characterization

Scanning Electron Microscopy of the samples were conducted with a JEOL 7800 F Field Emission Scanning Electron Microscope.

Output Measurement

The piezoelectric and hybrid output voltage signals were characterized using the Tektronix TDS1001B digital oscilloscope. The piezoelectric and hybrid devices' signals were further characterized by the VersaSTAT3 potentiostat; this device was used to analyze the potential of the piezoelectric and hybrid film as an energy harvester. This was done so by connecting the film with bridge rectifiers and capacitors and then analyzing their signals with the potentiostat. The current was measured using a Stanford Research System SR570 current pre amplifier.

Result and Discussion

Characterization of the Synthesized Nanocubes

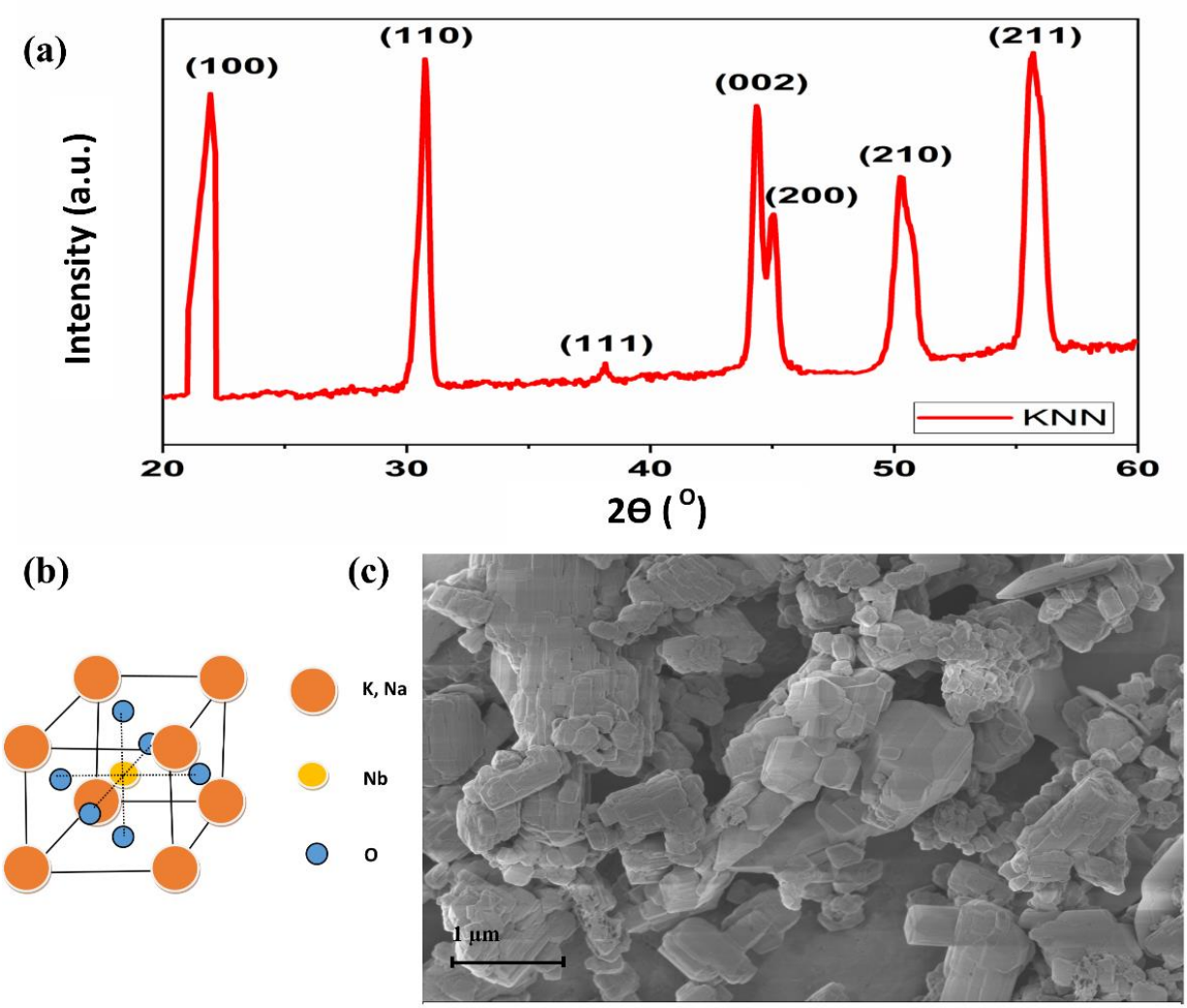

Figure 9: (a) X-ray Diffraction pattern of synthesized KNN powder. (b) Perovskite crystal structure of KNN (c) SEM image of KNN powder

Figure 9a shows the XRD pattern of synthesized KNN. Sharp peaks can be observed from the pattern at (100), (110), (002), (200) and (211) from 20° to 60° angle. These peaks

clearly denote the formation of perovskite crystalline structure (Fig 9b) of the KNN particles [119,120]. No impurities can be observed from K, Na or NbO_3 Besides, the sharp peaks of the pattern state the high crystalline quality of the KNN particles.

The KNN particles were also characterized using a Scanning Electron Microscopy (SEM). The results and the SEM image indicate that the KNN nano cubes of perovskite structure with orthorhombic phase have been synthesized. Diffraction peaks resulting from the impurities have been minimized with the high calcination temperature of 900^0 C. The sharp peaks and the peak split around $2\theta=45^0$ attribute to the purity of the KNN [121]. In addition to that, no pyrochlore phases are also detected. The structures of the KNN particles were further studied through SEM. Fig 9c shows the SEM image of the synthesized KNN particles in 1µm scale. The dimension of these synthesized cubic particles varied from 80nm to 300nm. The SEM also attributes to the higher grain uniformity and morphology compared to the KNN nanoparticles that have been produced in lower calcination temperatures [122]. Lower particle size could have been achieved by reducing the calcination temperature but that would have been achieved at the cost of losing grain uniformity and morphology [121].

Characterization of the KNN/PVDF/MWCNT based triboelectric and piezoelectric energy film

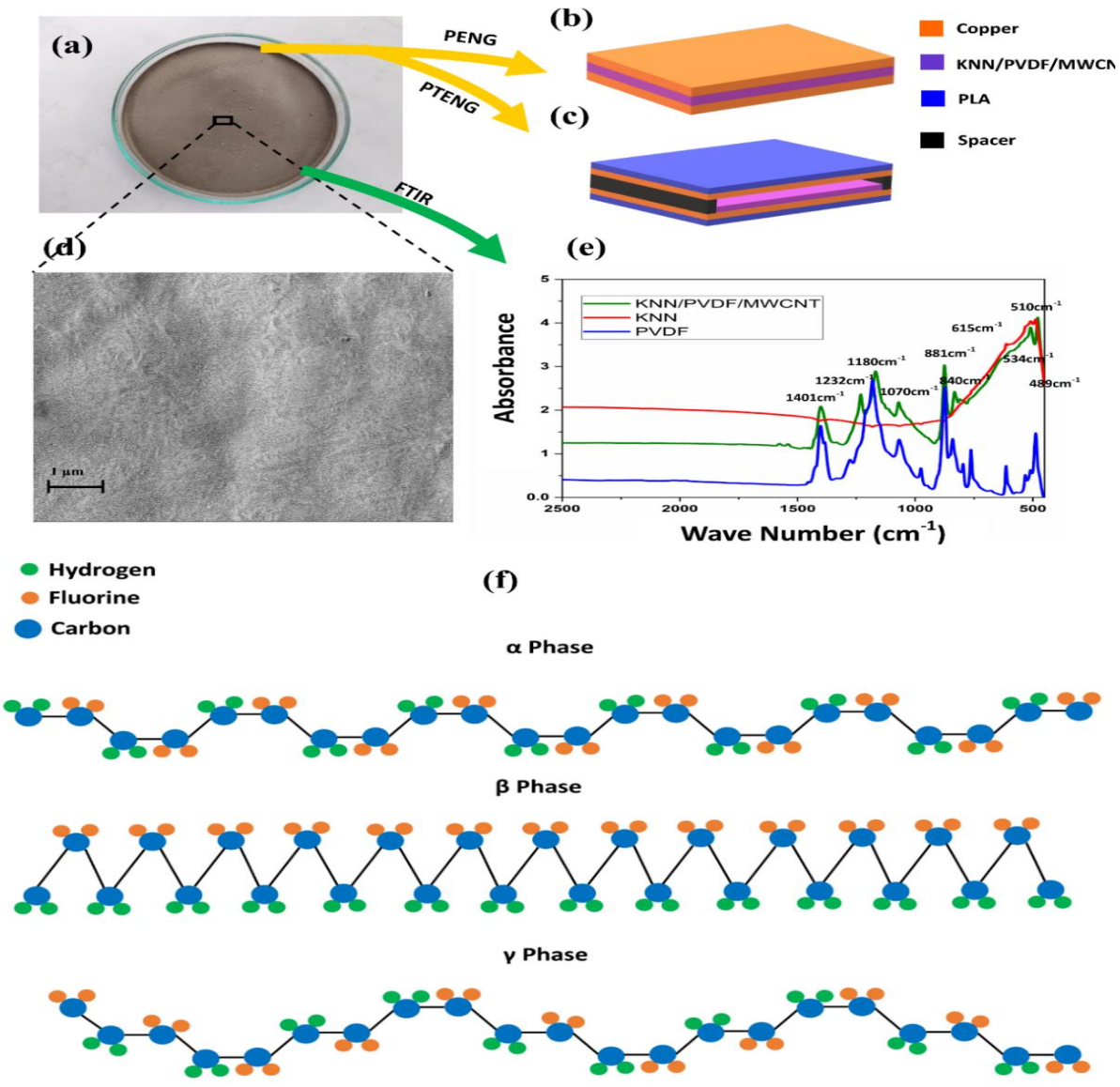

Figure 10: (a) Optical view of the synthesized KNN/PVDF/MWCNT film. Implementation of the energy film as (b) a PENG (c) Hybrid PTENG. (d) SEM image of the surface of the energy film (e) FTIR spectroscopy of the energy film (f) α , β and γ crystalline phases of PVDF

Figure 10a shows the optical image of the film composed of PVDF, KNN, and MWCNT. The EF can be used as PENG by attaching electrodes in both sides. The sandwiched EF along with the electrodes are shown in figure 10b. Copper has been used electrode in this experiment for their excellent conductivity and availability [123,124]. Additionally, a PTENG was synthesized with the EF (Figure 10c) by attaching the Cu electrode with on side of the film and attaching the other Cu electrode with a Polyurethane (PU) spacer of 1cm thickness. The whole PTENG structure is reinforced with the PLA layer added on top of the electrodes on both sides.

The surface morphology of the EF was studied with SEM. The SEM image of the film (Figure 10d) shows the uniformity of the film; It can be clearly seen in this image that the KNN and MWCNT has dispersed throughout the PVDF film making it uniform. Also, we do not see any KNN nanocubes on the surface of the film; this attributes to a better insertion of the KNN nanoparticles in the PVDF polymer matrix. Some black spots can be seen throughout the film, these represent the MWCNT.

Figure 10e shows the FTIR spectra for the pure PVDF film that we synthesized without adding KNN and MWCT, the KNN nanocubes, and the PVDF/KNN/MWCNT composite film. The sharp peaks observed at 881cm^{-1} and 1401cm^{-1} are due to the vibration of C-F stretching and C-H bending of PVDF [125,126]. The peaks around 1180cm^{-1} of the PVDF in the EF film indicates the presence of both β and γ crystalline phases at high intensity [127]. Besides,, the peaks at 510cm^{-1} , 840cm^{-1} and 1070cm^{-1} strongly corresponds to the presence of β phase [35,126,128]. Then we shift our focus on the peaks at 1232 cm^{-1} and 489 cm^{-1}. These peaks are exclusive for the indication of γ phase development [127,129]. It seems from the FTIR spectra that the sample is dominant on β phase with some hints of γ phase. The presence of β phase in the film is very significant for the piezoelectric effect [35]. The γ phase provides some stability

to the film as γ phase is more stable higher melting temperature that this enables the γ phase to stem the diminution of polarization over time [129,130]. The orientation in α , β and γ crystalline phases of PVDF are demonstrated in figure 10f. For the KNN, we see an emergence of a broad peak right under the wave number 1000 cm^{-1}; peaks on that region are characteristic vibration of the Nb-O octahedron which indicates the formation of a perovskite structure [131–134]. Finally, the peak of the composite film shows a superimposition of the peaks discussed above.

Piezoelectric Performance of the EF

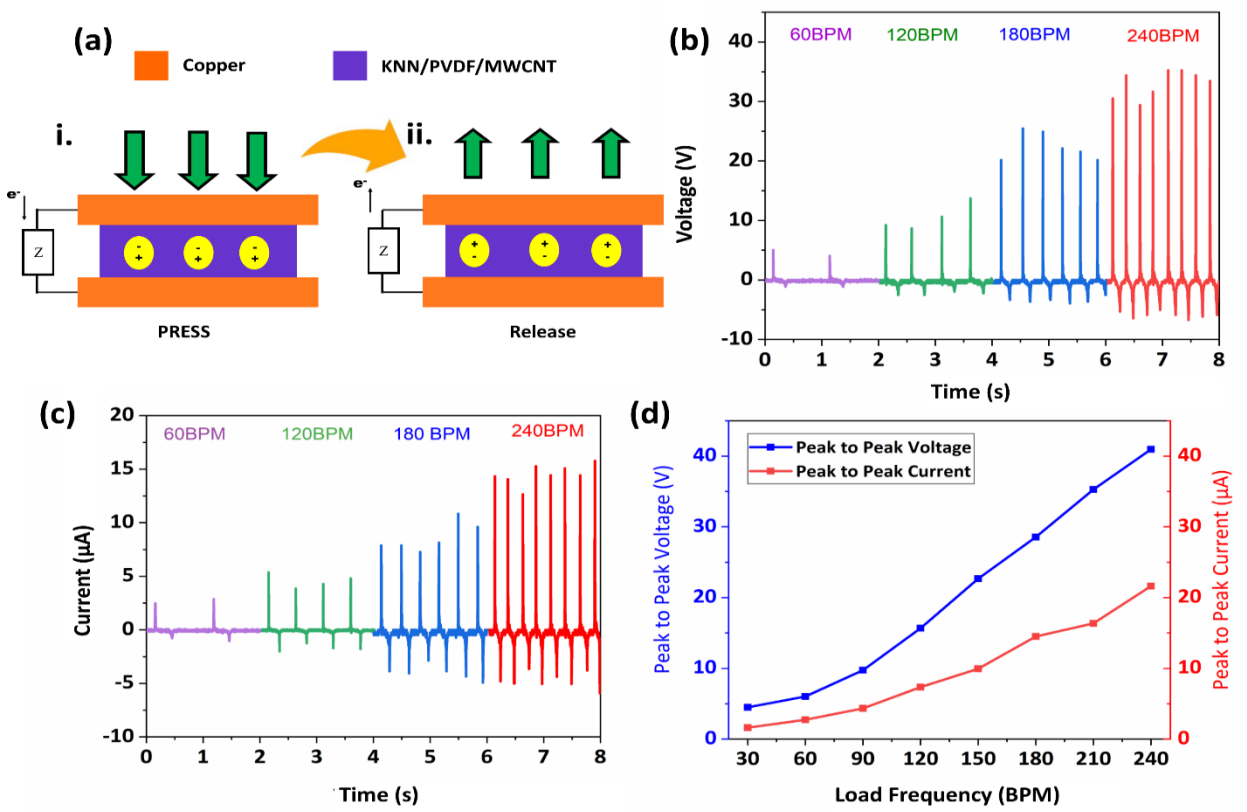

Figure 11: (a) Mechanism of the EF attached PENG i. Press stage ii. Release Stage (b) Output Voltage and (c) Current observed by tapping the EF attached PENG at 60 BPM, 120 BPM, 180 BPM and 240 BPM load frequency (d) Maximum peak to peak voltage and current observed for tapping the EF attached PENG at variable load frequencies.

The piezoelectric response of the EF was measured by applying external load on the EF attached PENG. Figure 11a demonstrates the working mechanism of the EF attached PENG under external pressure. When external vertical force is applied (Figure 11a-i) the crystal structure of KNN and PVDF gets interrupted. It results in orientation of electric dipole in the crystal structure. The orientation occurs in a direction which is known as stress induced poling effect [135,136]. An overall voltage difference emerges between two electrodes due to this orientation of dipoles. Positive voltage develops at the upper electrode due to attachment of the electrode with positive portion of the dipole. Electron moves from the upper electrode to the bottom electrode resulting a positive voltage signal in the output [48,137]. When the pressure is released from the PENG, the piezoelectric potential gets removed. As a result, electron moves from the bottom electrode to the upper, resulting a negative signal in the output [135,138]. The intensity of the positive peak was higher compared to the negative peak as the positive peak occurred due to the applied stress from the external source while the negative peak caused due to the resilience of the film by itself [139].

The output performance of the EF attached PENG was tested at 60 BPM (1 Hz), 120 BPM (2 Hz), 180 BPM (3 Hz) and 240 BPM (4 Hz) tapping frequency keeping 1 cm distance between the finger and the upper surface. Tapping acts as an external pressure on the device which results voltage and current signal in the output. Figure 11b and 11c demonstrates the output open circuit voltage and short circuit current by the EF attached PENG at variable load frequencies. Both the voltage and the current increases with increasing frequency. The maximum output voltage and current was observed to be 35.3 V and 15.8 μA for 240 BPM load frequency. Additionally, the maximum voltage for 60 BPM, 120 BPM and 180 BPM was observed to be 5

V, 13.7 V and 25.5 V. On the other hand, the maximum output current was recorded as 2.9 µA, 5.3 µA and 10.8 µA for the respective frequencies. With the increase of the load frequency the impact acceleration as well as the force applied on the PENG increases. This results in higher strain in the film which contributes to higher piezoelectric potential [140]. Also, the electrons have less time to neutralize the piezoelectric potential due to the increase of tapping frequency. Therefore, more charge accumulation occurs at the electrodes resulting higher electron flow and output current [141]. Figure 11d shows the maximum peak to peak output voltage and current by the PENG for a tapping frequency from 30 to 240 BPM. The maximum peak to peak voltage and current was noted to be 40.9 V and 21.6 µA respectively. The output signal increased at a lower rate for first 90 BPM lead frequency which increased linearly at a higher rate afterwards. Also, voltage increases at a higher slope compared to the current. This denotes the increasing resistance of the system with increase of load frequencies. Since the resistance of the conductor and electrode is a function of the mechanical dimension, the resistance changes with external force that increases with loading frequencies [142,143].

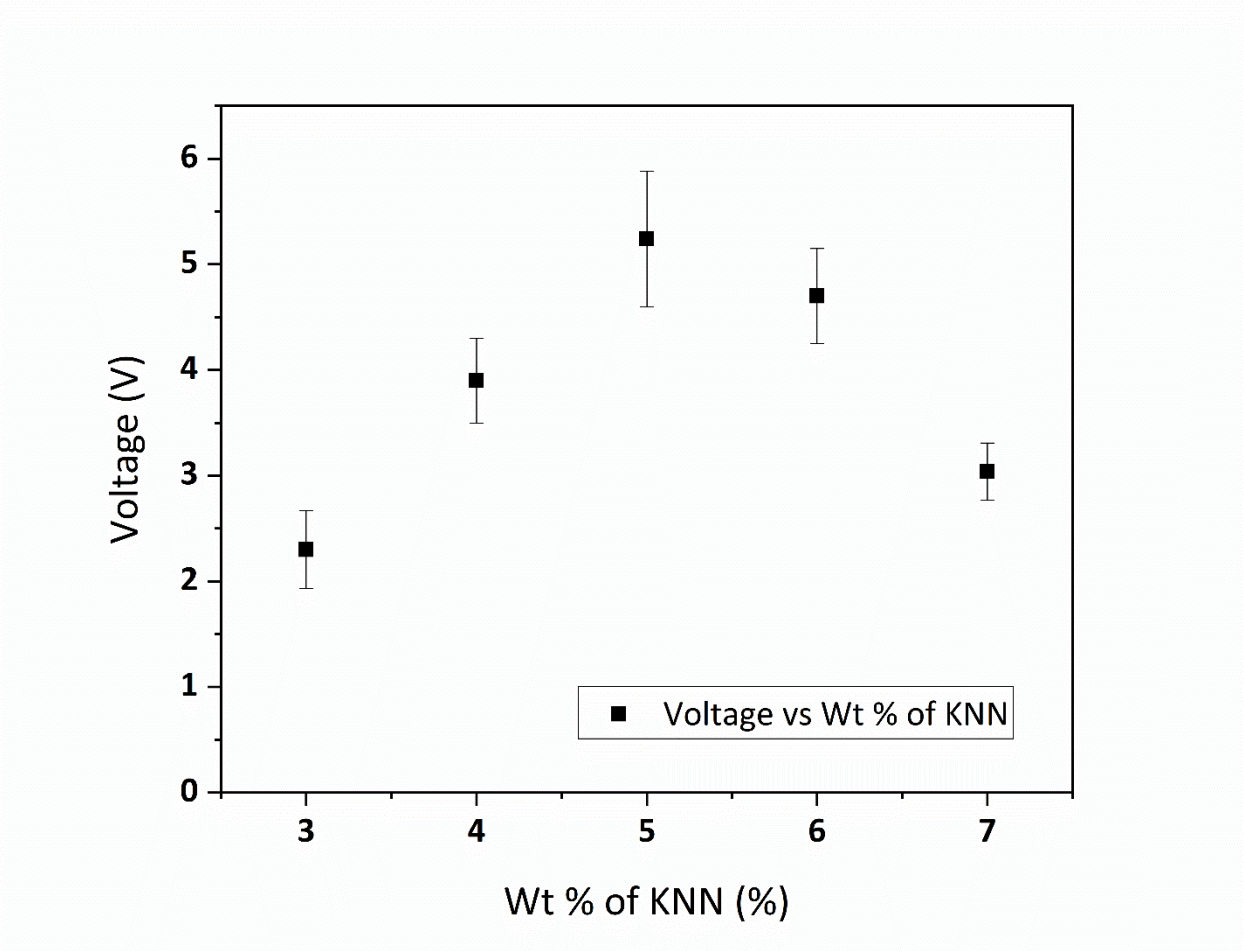

Figure 12: Maximum output voltage observed with the variable percentage of KNN in the EF by weight (Error bar for 95% Confidence Interval)

The Piezoelectric performance of the EF was also observed for variable percentage of KNN in the EF by weight. The EFs including 3% to 7% of KNN were used for this test. The EFs were tapped at 60 BPM load frequency with 1cm gap. Figure 12 shows the output voltage of EF with the increase of KNN in the EF. The maximum output voltage increased from 2.3 V to 5.24 V with the increase of KNN from 3% to 5%. However, the output decreased 3.04 V with further increase of KNN up to 7%. KNN act as a piezoelectric filler in the film. Increasing the

percentage of KNN in the film significantly effects the output. But, 5% of KNN in the EF, KNN contributes in restricting the nucleation of β crystallinity of the polymer and increases the chance of creating defects in the PVDF [144]. As a result, the output voltage decreased with the increase of KNN in the EF after 5 percent.

Performance of the EF as a pressure, force and finger motion sensor

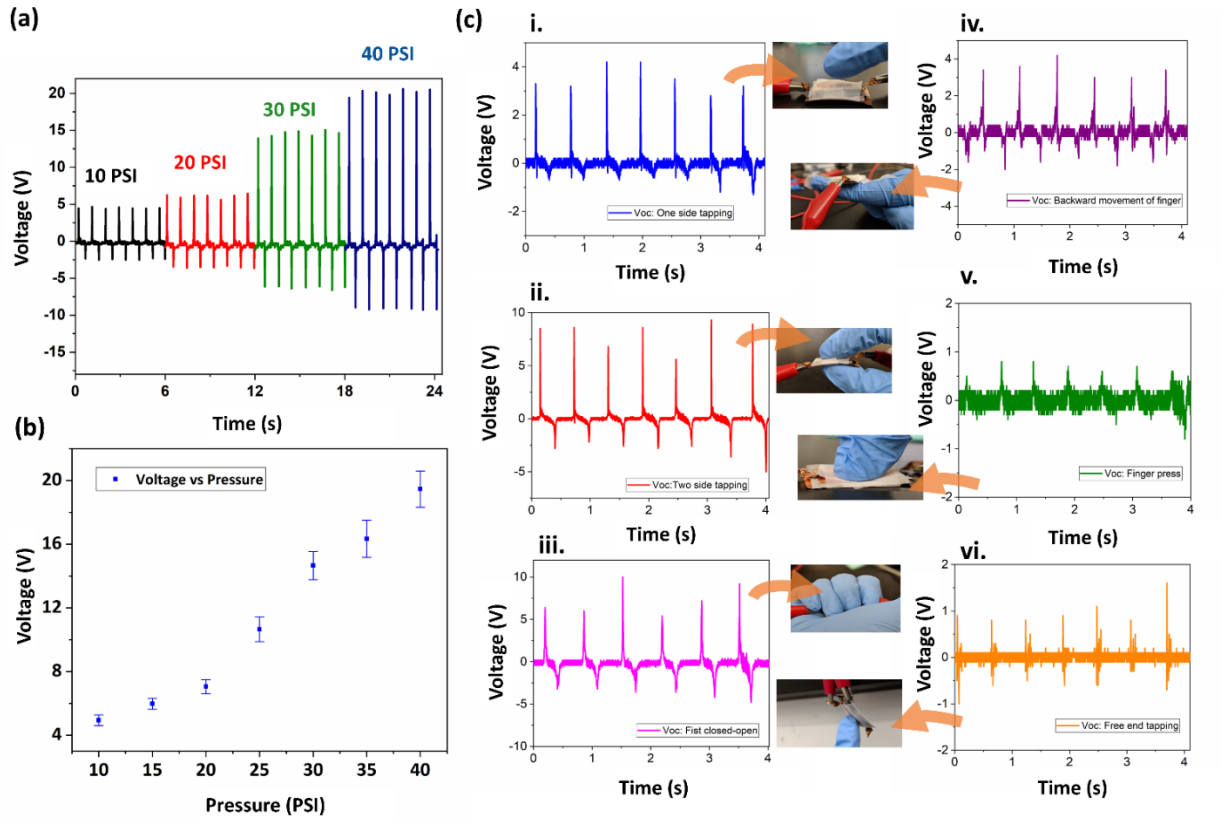

Figure 13: (a) Output piezoelectric voltage signal from the energy film at variable pressure of the pneumatic piston. (b) Maximum voltage observed at variable pressure (Error bars for 95% Confidence Interval of the mean) (c) Output piezoelectric voltage signal from the energy film different finger motion i. one side tapping ii. Two side taping iii. Fist closing and opening iv. backward movement of finger v. finger pressing without pulling the finger up vi. Free end tapping.

The response of the EF attached PENG was further tested for variable pressure. The test was performed at 75 BPM loading frequency with a pneumatic piston of 2cm diameter. The applied pressure varied from 10 PSI to 40 PSI. Supplementary Movie 1 shows the application of external load on the EF attached PENG with the pneumatic piston. The output voltage signals are demonstrated on figure 13a which clearly shows identical values of the output signal for certain pressure on the device. The maximum output voltage was observed to be 20.6V for 40 PSI Pneumatic pressure Figure 13b the resultant average value of the output voltage by the EF from 10 PSI to 40 PSI with 5 PSI interval. The error bars were considered for 95% Confidence Interval of the mean. The output voltage clearly increased as a non-linear function of the pressure. With the increase of the Pneumatic pressure the force on the EF also increases. The force value can be found by multiplying the pressure with the cross-sectional area of the piston. This increasing force results in the increase of compressive stress of the EF. Consequently, the strain of the EF increases which contributes to the higher piezoelectric voltage in the output. This identical increase of the output voltage with the pressure clearly supports the possible application of the EF as a pressure as well as force sensor.

Figure 4c shows the output signal by the EF under different finger motion. The device was directed towards different finger motions at 120 BPM. The strength and intensity of the touch and the vibration and direction of the motions helps the EF to distinguish between different finger motion [145–148]. This ability promotes its motion sensing operation. Figure 13c-i and 13c-ii demonstrates the output signal for tapping the EF attached from upper and both sides respectively. The maximum output voltage was observed for the two-side tapping was 9.3 V while it was 4.4 V for the single side tapping. The output voltage doubled due to the application of force from two sides. Besides, after the application of the stress, the relaxation of the films

occurs from both sides. As a result, the negative voltage was observed to be higher and sharper for the two-side tapping. In figure 13c-iii the signal represents the output signal from the EF in closes fist-open fist operation while keeping the device in the fist. The signal can be seen as identical with the signal related to two side tapping since the device was directed to force from both sides. The output voltage can be high as 10 V for this case. Next the PENG was attached in the back of the index finger and the finger was moved freely to backside at 120 BPM frequency. As the finger was attached with the lower electrode of the PENG, force was exerted on the lower electrode. This free movement to the back resulted a bending motion of the device. Negative voltage generates with every free movement of finger, which however, generates positive signal whenever the finger moves towards its initial position. The maximum output voltage was observed to be 4.2 V in this test. The signals are observed to be more vibrating compared to the double or single side tapping motions. Due to the free end of the motion, additional vibration can be observed through the signal during every cycle of the free movement [148,149]. The EF was also tested under continuous thumb press at 120 BPM without any distance of impact (Fig 13c-v). A single peak can observe for every press on the PENG. The maximum voltage of this continuous ‘w’ shaped response was 0.8 V. The zero distance of impact resulted in less force on the PENG which resulted low voltage in the output. Figure 4c-vi demonstrates the output response of the EF attached PENG under free end tapping. This can be more defined as a cantilever operation through the PENG. While tapping the film at free end, more vibration occurs in film due to cantilever action. This results in additional vibrations in the output response [149,150]. It can be clearly stated from the above discussion the EF shows identical response and intensity when directed to different finger motions. Therefore, it can be a potential sensor to detect biomechanical and finger motions. Different types biomechanical motions can be utilized

to power small electronic devices through this device. This can reduce the cost as well as complexity of the current devices. This also promotes its implementations in the wearable devices for sensory applications.

Output performance of EF attached Piezoelectric-Triboelectric Hybrid Nanogenerator

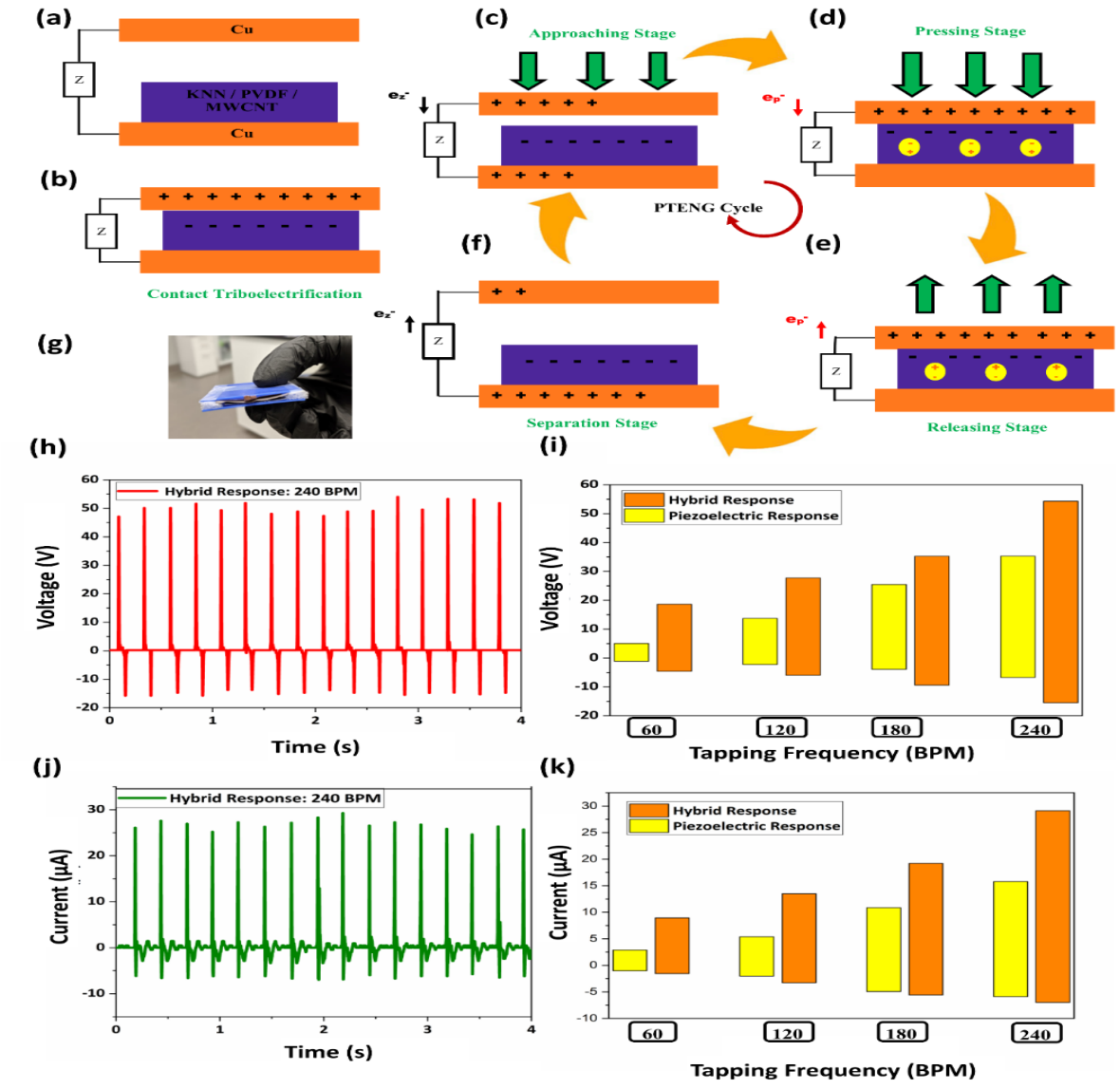

Figure 14: Working mechanism of the EF attached PTENG (a) EF attached hybrid PTENG at initial stage (b) EF attached PTENG in full contact due to external load (c) Approaching stage: Upper electrode of the EF attached PTENG starts approaching towards the EF due to the repetition of the external force (d) Pressing Stage: EF attached PTENG under fully pressed

condition (e) Releasing Stage: Pressure release from the EF attached PTENG due to the removal of external load (f) Separation Stage: Separation of the EF from the upper electrode as the electrode moves towards its initial position (g) Optical view of the EF attached PTENG (h) Output voltage response of the EF attached PTENG at 240 BPM tapping frequency (i) Comparison of the maximum peak to peak voltage between the EF attached PENG and PTENG at 60BPM, 120BPM, 180BPM and 240BPM tapping frequency (j) Output current response of the EF attached PTENG at 240 BPM tapping frequency (k) Comparison of the maximum peak to peak current between the EF attached PENG and PTENG at 60BPM, 120BPM, 180BPM and 240BPM tapping frequency

Figure 14a to 14g demonstrates the triboelectric working mechanism of the EF attached PTENG. The triboelectric function of the device occurs due to contact triboelectrification and electrostatic induction [15,104,151] The charge neutral initial stage of the device with full airgap is shown at figure 14a. With the application of external force on the device the upper layer of Cu moves towards the EF. The Cu layer gets in full contact with the EF (Fig 14b). Due to the lower position of PVDF in the triboelectric series compared to Cu, electrons transfer to the PVDF surface from Cu surface which is defined as contact triboelectrification [4,152,153]. The upper electrode moves backs to its initial position. The PTENG circle starts operating after the upper electrode of the device starts approaching towards the EF after contact triboelectrification (Fig 14c). While the upper electrode is moving towards the EF, an electron flow occurs from the upper electrode towards the lower one due to the potential difference between two electrodes as a result of electrostatic induction. The upper electrode then comes in full contact with the EF again. The upper electrode is positively charged at this stage to counterbalance the negatively charged EF film. At this stage, the EF goes under full pressure due to the external load (Fig 14d).

The Piezoelectric dipoles are created at this pressing stage which has been discussed in the previous sections. Electron moves from upper electrode to the lower electrode due to the piezoelectric voltage. The device shows maximum positive voltage in the output at this position. At the next stage, the external load is withdrawn from the device. As a result, the piezoelectric potential is removed from the device that leads towards flow of electron from the bottom electrode to the upper electrode (Fig 14e). The output voltage starts decreasing at this point. Eventually, The Cu layer starts to move back towards its initial position due to this release of the external force (Fig 14f). To neutralize electrostatic voltage between two electrodes, electron from the bottom electrode moves towards the positively charged upper electrode. The whole cycle results in an Alternative Current (AC) in the output which continues with the application of external force. An optical view of the PTENG is demonstrated at figure 14g.

The hybrid response by the EF attached PTENG at 240 BPM is demonstrated at figure 14h. The air gap between the finger and the device was set as 1cm. The maximum output and peak to peak voltage of the device was noted as 54.1 V and 69.4V respectively. The maximum peak to peak voltage of the hybrid PTENG was compared with maximum peak to peak voltage by the PENG at figure 14i. The maximum output voltage for the PTENG was 18.6 V, 27.7 V and 35.2 V for the PTENG at 60 BPM, 120 BPM and 180 BPM load frequencies which came as 5 V, 13.7 V and 25.5 V for the PENG. The maximum voltage of the PTENG was higher compared to the PENG alone. The combined effect of triboelectricity and piezoelectricity resulted in 18.8 V higher output open circuit voltage compared to the piezoelectric voltage alone at 240 BPM. This difference increased clearly with increased load frequency. Also, the short circuit current showed the similar trend for the increasing load frequencies. Figure 14j shows the output current by the EF attached PTENG for 240 BPM load frequency. The maximum short circuit current was

observed to be 29.4μA. The maximum peak to peak current by the EF attached PTENG was also compared with the output current response by the PENG at figure 14k. The output current for the PTENG increased from 8.9 μA to 29.1 μA with the increase of load frequencies from 60 BPM to 240 BPM. The device is struck at higher kinetic energy with higher loading frequency due to the increase of higher loading frequencies. This higher kinetic energy contributes in the flow of electron [151]. Besides, the electrons flows at a shorter time to neutralize charge accumulation which results in higher output current [154]. The voltage also increases with the increasing loading frequencies as a linear function of current. [100,101]. The higher triboelectric output with higher frequencies significantly contributes in the increase of output for the PTENG at a higher rate compared to the output by the PENG.

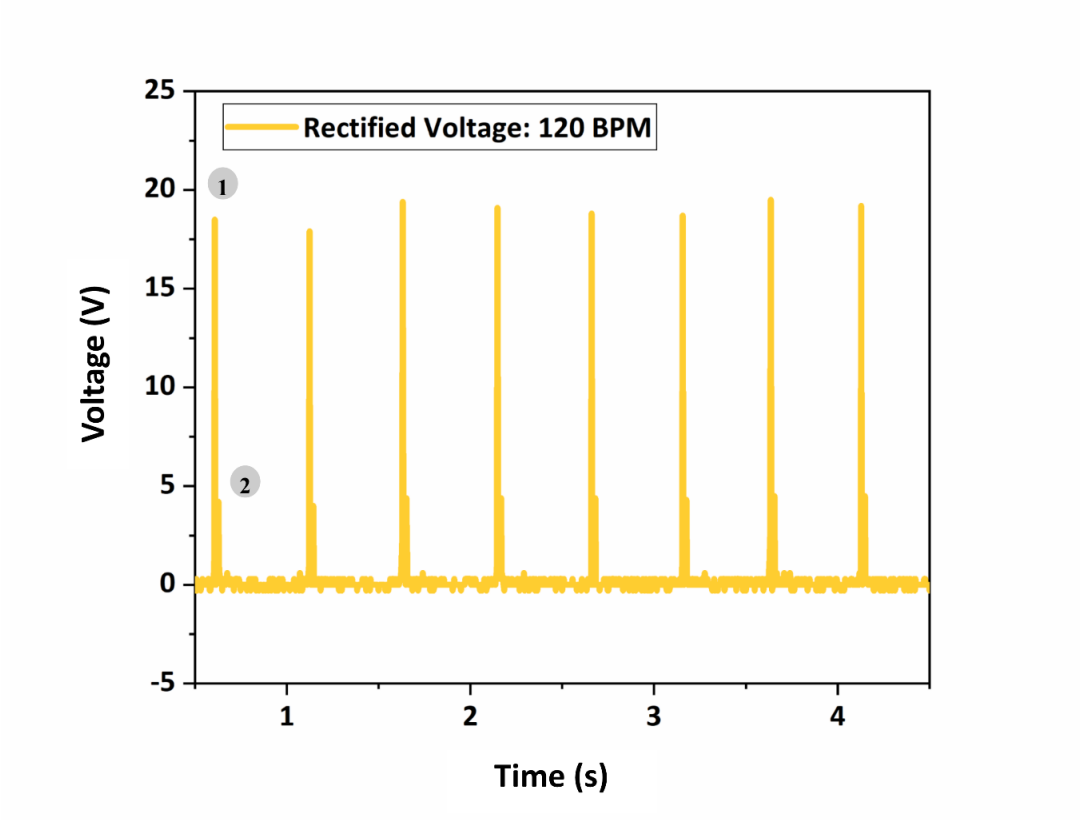

Figure 15: Rectified voltage signal by EF attached hybrid PTENG at 120 BPM loading frequency.

The performance of the EF attached was further tested with conventional electronic components. First, it was tested with a full wave bridge rectifier at 120 BPM and loading voltage and 1cm finger to device distance. Figure 15 shows the rectified output signal by the PTENG. The signal by the PTENG was completely rectified by the bridge rectifier. Point 1 and 2 indicates towards the signal regarding pressing the releasing the EF attached PTENG respectively after the rectifying operation. The maximum voltage after rectifying the voltage was noted as 18.4 V.

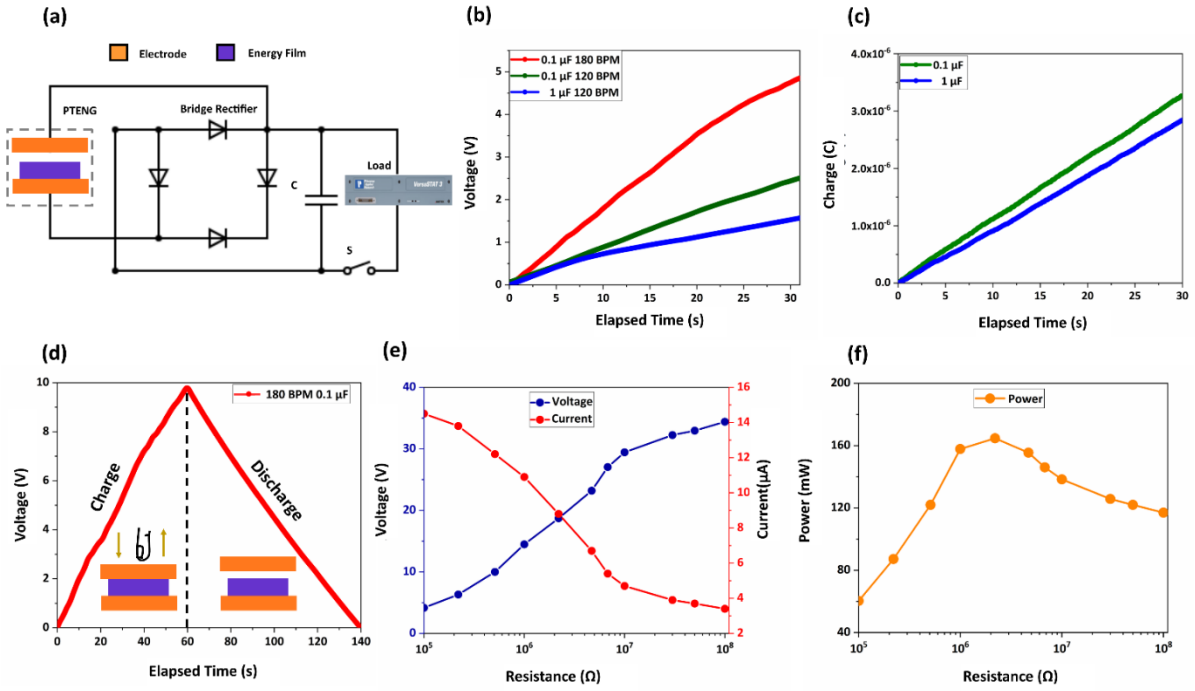

Figure 16: (a) Electrical circuit used for charging the Capacitors for EF attached PTENG (b) Charging capacitors for 30s with EF attached PTENG through finger tapping (c) Observed accumulated charge during charging the 0.1µF and 1µF capacitors by tapping the EF attached PTENG. (d) Charging and Discharging of 0.1µF capacitors with EF attached PTENG (e) Average Voltage and Current measured with variable external resistance with EF attached PTENG (f) Average Power measured with variable external resistance with EF attached PTENG

In another experiment the EF attached PTENG was capacitors for analyzing its capability to harvest and store energy from mechanical motions and provide constant biased voltage for powering electronic devices [107,110]. The circuitry system used for the test is exhibited at figure 16a. The device was connected with a full wave bridge rectifier followed by a parallel connection with a capacitor. The VersaStat3 was basically used to this test. Figure 16b shows the

output by the PTENG while charging 0.1µF and 1µF capacitors at 120 BPM and 180 BPM loading frequencies for 30s. The maximum voltage after charging the 0.1 µF and 1 µF capacitors at 120 BPM loading frequency was 2.5 V and 1.6 V respectively. Higher capacitor leads towards higher loss of charges in the capacitor [28,111,155,156]. Therefore, higher voltage was observed for 0.1 µF capacitor. Besides, the 0.1µF charged at a higher rate at 180 BPM compared to 120 BPM frequency. The maximum voltage after 30s for 180 BPM loading was observed to be 4.9 V. The larger number of contacts between the surface due to the higher frequency of loading leads towards higher transfer of charges. As a result, higher output voltage as well as higher rate of charging can be observed[151,156]. In addition, the accumulated number of charges at the output during the test was observed for 0.1µF and 1µF capacitors (Fig 16c). The charge accumulation in the output increased linearly with time. The number of accumulated charges in the output for 0.1 µF and 1 µF capacitors at 120 BPM was 3.2 µC and 2.8 µC respectively. The higher loss of charge in 1 µF capacitor leads toward lower accumulation of charge in the output. Subsequently, the 0.1 µF capacitor used for a charging-discharging test with the PTENG (Fig 16d). It was frequently tapped for 60s at 180 BPM. It reached up to 9.8V after 60s (180 cycles). The load was released afterwards. The device took about 80s to discharge. The charging of the device fully depends on the tapping force and frequency , however the discharge of the capacitor occurs at a constant rate as there is no external force during discharge [156]. The above results clearly indicate the application of the EF attached PTENG for self-charging operations of electronic devices.

The PTENG was further characterized with external resistance from 10^4 to 10^8 Ω. The output voltage and current for variable external load is presented at figure 16e. Following the Ohm's law (V = IR) the voltage increases and the current decreases with the increase of

resistance. The voltage and current incidents at 2.2 MΩ, which can be defined as the optimum point. The power is expected to maximize at this optimum resistance [157,158]. Figure 16f shows the measured output power for variable external load. The maximum power measured was 164.74 mW at 2.2 MΩ (Optimum point) external resistance.

EF and Kapton based PTENG

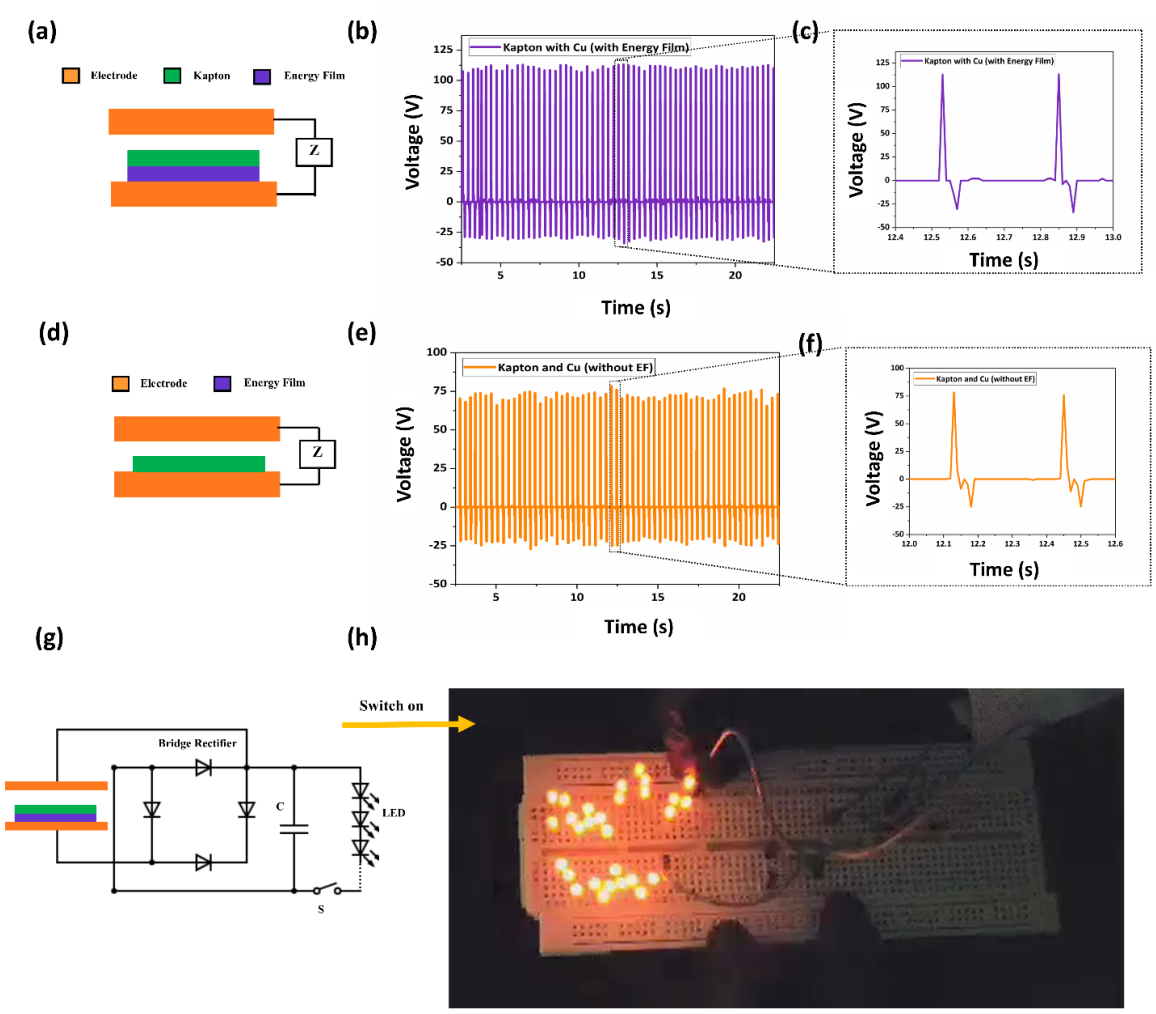

Figure 17: (a) Schematic of the Nanogenerator with the Cu, Kapton and Energy Film (b) Output voltage of the EF attached Kapton based PTENG at 180 BPM (c) Extended view of the output voltage of the PTENG from 12.4s to 13s (d) Schematic of the Nanogenerator with Cu and Kapton € Output voltage of the TENG without EF at 180 BPM (f) Extended view of the output voltage of the PTENG from 12s to 12.6s (g) Electrical circuit used for powering LEDs (h) Lighting LEDs with the EF attached Kapton based PTENG

The EF was further attached with Kapton to fabricate a PTENG for higher output. Kapton is highly known for its triboelectric properties [159,160] The Kapton layer is set over the EF layer along with the Cu electrodes (Fig 17a). The device was tapped at 180 BPM frequency. The output shows a maximum voltage of 113.2 V (Figure 17b). An extended view of the voltage signals is demonstrated at figure 17c. A Kapton based Triboelectric Nanogenerator (TENG) was also constructed for comparison purpose (Fig 17d). The Kapton based TENG exhibited a maximum 78.4 V for the same experimental condition. The figure 17e shows the output signal for Kapton based TENG. The extended view of the output signal by the TENG was presented at figure 17f. It can be clearly stated that the EF is compatible with a Kapton layer to fabricate a PTENG. More importantly, the PTENG shows higher output compared to Kapton based TENG due to the combination of piezoelectricity and triboelectricity from the EF and Kapton respectively.

The EF/Kapton based PTENG was further utilized to test with Light Emitting Diodes (LED). An equivalent circuitry diagram has been demonstrated on figure 17g. The circuit included a bridge rectifier, capacitors and a switch. The LEDs were connected in series. The circuit was switched on after tapping the device for 60s at 120 BPM. 30 LEDs were successfully lightening after switching on the circuit (Figure 17h). It is evident from the experiment that the EF has a huge prospective component to power small electronic devices. Also, the mechanical energy harvesting capability and sensory characteristics of the piezoelectric and triboelectric EF magnifies its application in self-powered sensory devices. Proper application of the EF will promote the goal of led free energy harvesting and lead towards sustainable development.

Conclusion

In Summary, KNN nanocube was synthesized using ball milling method to fabricate a Piezoelectric and triboelectric hybrid energy film along with PVDF and MWCNT. The EF provided a maximum piezoelectric voltage and current of 35.3 V and 15.8 µA respectively. The film was observed to be sensitive for variable pressure and force. Besides, the energy film was sensitive to various finger motion. The results promote the application of this energy film as a pressure, force and motion sensor. The film also showed higher output voltage with the increase of the percentage of KNN up to 5% by weight. The film was successfully utilized as piezoelectric/triboelectric hybrid nanogenerator for higher output voltage. The maximum voltage and current during the hybridization were noted as 54.1V and 29.4 µA. The output voltage was observed to be 28.8 V higher compared to the previous studies regarding KNN and PVDF due to the utilization of both triboelectricity and piezoelectricity. Furthermore, the energy film was successfully integrated with bridge rectifiers, capacitors and LEDs. The energy film showed the capability of charging capacitors of 0.1µF and 1µF. The optimum power for the film was measured to be 164.74 mW with 2.2MΩ load resistance. Additionally, the attachment of Kapton with the energy film showed a high voltage of 113.2 V. 30 LEDs were lightened with this modified device. Overall, this film is a potential medium for lead free mechanical energy harvesting in a sustainable way.

REFERENCES

[1] I. Hussain, H.P. Tran, J. Jaksik, J. Moore, N. Islam, M.J. Uddin, Functional materials, device architecture, and flexibility of perovskite solar cell, Emergent Mater. 1 (2018) 133–154. https://doi.org/10.1007/s42247-018-0013-1.

[2] N. Abas, A. Kalair, N. Khan, Review of fossil fuels and future energy technologies, Futures. 69 (2015) 31–49. https://doi.org/10.1016/j.futures.2015.03.003.

[3] A.M. Abdullah, A.R. Chowdhury, Y. Yang, H. Vasquez, H.J. Moore, J.G. Parsons, K. Lozano, J.J. Gutierrez, K.S. Martirosyan, M.J. Uddin, Tailoring the viscosity of water and ethylene glycol based TiO2 nanofluids, Journal of Molecular Liquids. 297 (2020) 111982. https://doi.org/10.1016/j.molliq.2019.111982.

[4] A.R. Chowdhury, A.M. Abdullah, I. Hussain, J. Lopez, D. Cantu, S.K. Gupta, Y. Mao, S. Danti, M.J. Uddin, Lithium doped zinc oxide based flexible piezoelectric-triboelectric hybrid nanogenerator, Nano Energy. 61 (2019) 327–336. https://doi.org/10.1016/j.nanoen.2019.04.085.

[5] N. Espinosa, M. Hösel, D. Angmo, F. C. Krebs, Solar cells with one-day energy payback for the factories of the future, Energy & Environmental Science. 5 (2012) 5117–5132. https://doi.org/10.1039/C1EE02728J.

[6] L. Lin, S. Wang, S. Niu, C. Liu, Y. Xie, Z.L. Wang, Noncontact Free-Rotating Disk Triboelectric Nanogenerator as a Sustainable Energy Harvester and Self-Powered

Mechanical Sensor, ACS Appl. Mater. Interfaces. 6 (2014) 3031–3038. https://doi.org/10.1021/am405637s.

[7] M.S. Dresselhaus, I.L. Thomas, Alternative energy technologies, Nature. 414 (2001) 332–337. https://doi.org/10.1038/35104599.

[8] E. Koçak, A. Şarkgüneşi, The renewable energy and economic growth nexus in Black Sea and Balkan countries, Energy Policy. 100 (2017) 51–57. https://doi.org/10.1016/j.enpol.2016.10.007.

[9] Z.L. Wang, J. Song, Piezoelectric Nanogenerators Based on Zinc Oxide Nanowire Arrays, Science. 312 (2006) 242–246. https://doi.org/10.1126/science.1124005.

[10] P.K. Panda, Review: environmental friendly lead-free piezoelectric materials, J Mater Sci. 44 (2009) 5049–5062. https://doi.org/10.1007/s10853-009-3643-0.

[11] F.-R. Fan, Z.-Q. Tian, Z. Lin Wang, Flexible triboelectric generator, Nano Energy. 1 (2012) 328–334. https://doi.org/10.1016/j.nanoen.2012.01.004.

[12] Q. Zheng, B. Shi, Z. Li, Z.L. Wang, Recent Progress on Piezoelectric and Triboelectric Energy Harvesters in Biomedical Systems, Adv Sci (Weinh). 4 (2017) 1700029. https://doi.org/10.1002/advs.201700029.

[13] B.J. Hansen, Y. Liu, R. Yang, Z.L. Wang, Hybrid Nanogenerator for Concurrently Harvesting Biomechanical and Biochemical Energy, ACS Nano. 4 (2010) 3647–3652. https://doi.org/10.1021/nn100845b.

[14] M. Han, X. Zhang, W. Liu, X. Sun, X. Peng, H. Zhang, Low-frequency wide-band hybrid energy harvester based on piezoelectric and triboelectric mechanism, Sci. China Technol. Sci. 56 (2013) 1835–1841. https://doi.org/10.1007/s11431-013-5270-x.

[15] P. Bai, G. Zhu, Z.-H. Lin, Q. Jing, J. Chen, G. Zhang, J. Ma, Z.L. Wang, Integrated Multilayered Triboelectric Nanogenerator for Harvesting Biomechanical Energy from Human Motions, ACS Nano. 7 (2013) 3713–3719. https://doi.org/10.1021/nn4007708.

[16] A.R. Chowdhury, A.M. Abdullah, U.V. Romero, I. Hussain, C. Olivares, S. Danti, J. Li, M.J. Uddin, Decentralized Triboelectric Electronic Health Monitoring Flexible Microdevice, MEDICAL DEVICES & SENSORS. n/a (2020) e10103. https://doi.org/10.1002/mds3.10103.

[17] L. Jin, J. Tao, R. Bao, L. Sun, C. Pan, Self-powered Real-time Movement Monitoring Sensor Using Triboelectric Nanogenerator Technology, Scientific Reports. 7 (2017) 1–6. https://doi.org/10.1038/s41598-017-10990-y.

[18] Z. Lou, L. Li, L. Wang, G. Shen, Recent Progress of Self-Powered Sensing Systems for Wearable Electronics, Small. 13 (2017) 1701791. https://doi.org/10.1002/smll.201701791.

[19] A.R. Chowdhury, J. Jaksik, I. Hussain, R. Longoria, O. Faruque, F. Cesano, D. Scarano, J. Parsons, M.J. Uddin, Multicomponent nanostructured materials and interfaces for efficient piezoelectricity, Nano-Structures & Nano-Objects. 17 (2019) 148–184. https://doi.org/10.1016/j.nanoso.2018.12.002.

[20] W.-S. Jung, M.-G. Kang, H.G. Moon, S.-H. Baek, S.-J. Yoon, Z.-L. Wang, S.-W. Kim, C.-Y. Kang, High Output Piezo/Triboelectric Hybrid Generator, Scientific Reports. 5 (2015) 1–6. https://doi.org/10.1038/srep09309.

[21] Y. Xi, J. Wang, Y. Zi, X. Li, C. Han, X. Cao, C. Hu, Z. Wang, High efficient harvesting of underwater ultrasonic wave energy by triboelectric nanogenerator, Nano Energy. 38 (2017) 101–108. https://doi.org/10.1016/j.nanoen.2017.04.053.

[22] F. Liu, Y. Liu, Y. Lu, Z. Wang, Y. Shi, L. Ji, J. Cheng, Electrical analysis of triboelectric nanogenerator for high voltage applications exampled by DBD microplasma, Nano Energy. 56 (2019) 482–493. https://doi.org/10.1016/j.nanoen.2018.11.064.

[23] A.M. Abdullah, A. Flores, A.R. Chowdhury, J. Li, Y. Mao, M.J. Uddin, Synthesis and fabrication of self-sustainable triboelectric energy case for powering smart electronic devices, Nano Energy. 73 (2020) 104774. https://doi.org/10.1016/j.nanoen.2020.104774.

[24] W. Tang, T. Jiang, F.R. Fan, A.F. Yu, C. Zhang, X. Cao, Z.L. Wang, Liquid-Metal Electrode for High-Performance Triboelectric Nanogenerator at an Instantaneous Energy Conversion Efficiency of 70.6%, Advanced Functional Materials. 25 (2015) 3718–3725. https://doi.org/10.1002/adfm.201501331.

[25] Z.L. Wang, Triboelectric nanogenerators as new energy technology and self-powered sensors – Principles, problems and perspectives, Faraday Discuss. 176 (2015) 447–458. https://doi.org/10.1039/C4FD00159A.

[26] H.H. Singh, N. Khare, Flexible ZnO-PVDF/PTFE based piezo-tribo hybrid nanogenerator, Nano Energy. 51 (2018) 216–222. https://doi.org/10.1016/j.nanoen.2018.06.055.

[27] W. Wang, J. Zhang, Y. Zhang, F. Chen, H. Wang, M. Wu, H. Li, Q. Zhu, H. Zheng, R. Zhang, Remarkably enhanced hybrid piezo/triboelectric nanogenerator via rational modulation of piezoelectric and dielectric properties for self-powered electronics, Appl. Phys. Lett. 116 (2020) 023901. https://doi.org/10.1063/1.5134100.

[28] Simiao Niu, Ying Liu, Yu Sheng Zhou, Sihong Wang, Long Lin, Zhong Lin Wang, Optimization of Triboelectric Nanogenerator Charging Systems for Efficient Energy Harvesting and Storage, IEEE Trans. Electron Devices. 62 (2015) 641–647. https://doi.org/10.1109/TED.2014.2377728.

[29] A.M. Abdullah, A. Flores, A.R. Chowdhury, J. Li, Y. Mao, M.J. Uddin, Synthesis and fabrication of self-sustainable triboelectric energy case for powering smart electronic devices, Nano Energy. 73 (2020) 104774. https://doi.org/10.1016/j.nanoen.2020.104774.

[30] H.B. Kang, C.S. Han, J.C. Pyun, W.H. Ryu, C.-Y. Kang, Y.S. Cho, (Na,K)NbO3 nanoparticle-embedded piezoelectric nanofiber composites for flexible nanogenerators, Composites Science & Technology. 111 (2015) 1–8. https://doi.org/10.1016/j.compscitech.2015.02.015.

[31] Organic-Inorganic Hybrid Materials for Piezoelectric/Triboelectric Nanogenerator - ProQuest, (n.d.). https://search.proquest.com/openview/a47c506d20c98e8e9bbd4586b7f37bce/1?pq-origsite=gscholar&cbl=18750&diss=y (accessed January 13, 2020).

[32] Q. Jing, S. Kar-Narayan, Nanostructured polymer-based piezoelectric and triboelectric materials and devices for energy harvesting applications, J. Phys. D: Appl. Phys. 51 (2018) 303001. https://doi.org/10.1088/1361-6463/aac827.

[33] Y. Koseki, K. Aimi, S. Ando, Crystalline structure and molecular mobility of PVDF chains in PVDF/PMMA blend films analyzed by solid-state 19 F MAS NMR spectroscopy, Polymer Journal. 44 (2012) 757–763. https://doi.org/10.1038/pj.2012.76.

[34] (15) Piezoelectricity in PVDF and PVDF Based Piezoelectric Nanogenerator: A Concept | Request PDF, (n.d.). https://www.researchgate.net/publication/317153707_Piezoelectricity_in_PVDF_and_PVDF_Based_Piezoelectric_Nanogenerator_A_Concept (accessed May 8, 2020).

[35] L. Ruan, X. Yao, Y. Chang, L. Zhou, G. Qin, X. Zhang, Properties and Applications of the β Phase Poly(vinylidene fluoride), Polymers (Basel). 10 (2018). https://doi.org/10.3390/polym10030228.

[36] S. Yu, W. Zheng, W. Yu, Y. Zhang, Q. Jiang, Z. Zhao, Formation Mechanism of β-Phase in PVDF/CNT Composite Prepared by the Sonication Method, Macromolecules. 42 (2009) 8870–8874. https://doi.org/10.1021/ma901765j.

[37] G.H. Kim, S.M. Hong, Y. Seo, Piezoelectric properties of poly(vinylidene fluoride) and carbon nanotube blends: beta-phase development, Phys Chem Chem Phys. 11 (2009) 10506–10512. https://doi.org/10.1039/b912801h.

[38] S. Kim, Y. Song, M.J. Heller, Influence of MWCNTs on β-Phase PVDF and Triboelectric Properties, Journal of Nanomaterials. 2017 (2017) e2697382. https://doi.org/10.1155/2017/2697382.

[39] Lithium doped zinc oxide based flexible piezoelectric-triboelectric hybrid nanogenerator - ScienceDirect, (n.d.). https://www.sciencedirect.com/science/article/abs/pii/S2211285519303866 (accessed May 8, 2020).

[40] R. Guo, Y. Guo, H. Duan, H. Li, H. Liu, Synthesis of Orthorhombic Perovskite-Type ZnSnO3 Single-Crystal Nanoplates and Their Application in Energy Harvesting, ACS Appl. Mater. Interfaces. 9 (2017) 8271–8279. https://doi.org/10.1021/acsami.6b16629.

[41] X. Chen, S. Xu, N. Yao, Y. Shi, 1.6 V Nanogenerator for Mechanical Energy Harvesting Using PZT Nanofibers, Nano Lett. 10 (2010) 2133–2137. https://doi.org/10.1021/nl100812k.

[42] K.-I. Park, J.H. Son, G.-T. Hwang, C.K. Jeong, J. Ryu, M. Koo, I. Choi, S.H. Lee, M. Byun, Z.L. Wang, K.J. Lee, Highly-Efficient, Flexible Piezoelectric PZT Thin Film Nanogenerator on Plastic Substrates, Advanced Materials. 26 (2014) 2514–2520. https://doi.org/10.1002/adma.201305659.

[43] X. Lu, H. Qu, M. Skorobogatiy, Piezoelectric Micro- and Nanostructured Fibers Fabricated from Thermoplastic Nanocomposites Using a Fiber Drawing Technique: Comparative Study and Potential Applications, ACS Nano. 11 (2017) 2103–2114. https://doi.org/10.1021/acsnano.6b08290.

[44] X. Lu, H. Qu, M. Skorobogatiy, Piezoelectric Microstructured Fibers via Drawing of Multimaterial Preforms, Scientific Reports. 7 (2017) 1–12. https://doi.org/10.1038/s41598-017-01738-9.

[45] Y. Shiratori, A. Magrez, W. Fischer, C. Pithan, R. Waser, Temperature-induced Phase Transitions in Micro-, Submicro-, and Nanocrystalline NaNbO 3, The Journal of Physical Chemistry C. 111 (n.d.) 18493–18502.

[46] T.-Y. Ke, H.-A. Chen, H.-S. Sheu, J.-W. Yeh, H.-N. Lin, C.-Y. Lee, H.-T. Chiu, Sodium Niobate Nanowire and Its Piezoelectricity, J. Phys. Chem. C. 112 (2008) 8827–8831. https://doi.org/10.1021/jp711598j.

[47] A. Teka, S. Bairagi, M. Shahadat, M. Joshi, S.Z. Ahammad, S.W. Ali, Poly(vinylidene fluoride) (PVDF)/potassium sodium niobate (KNN)–based nanofibrous web: A unique nanogenerator for renewable energy harvesting and investigating the role of KNN nanostructures, Polymers for Advanced Technologies. 29 (2018) 2537–2544. https://doi.org/10.1002/pat.4365.

[48] S. Bairagi, S.W. Ali, Influence of High Aspect Ratio Lead-Free Piezoelectric Fillers in Designing Flexible Fibrous Nanogenerators: Demonstration of Significant High Output Voltage, Energy Technology. 7 (2019) 1900538. https://doi.org/10.1002/ente.201900538.

[49] S. Bairagi, S.W. Ali, Flexible lead-free PVDF/SM-KNN electrospun nanocomposite based piezoelectric materials: Significant enhancement of energy harvesting efficiency of the nanogenerator, Energy. 198 (2020) 117385. https://doi.org/10.1016/j.energy.2020.117385.

[50] S. Bairagi, S.W. Ali, Investigating the role of carbon nanotubes (CNTs) in the piezoelectric performance of a PVDF/KNN-based electrospun nanogenerator, Soft Matter. 16 (2020) 4876–4886. https://doi.org/10.1039/D0SM00438C.

[51] E. Jovanov, A. Milenkovic, C. Otto, P.C. de Groen, A wireless body area network of intelligent motion sensors for computer assisted physical rehabilitation, Journal of NeuroEngineering and Rehabilitation. 2 (2005) 6. https://doi.org/10.1186/1743-0003-2-6.

[52] P.-J. (John) Hsu, Portable cell phone battery charger using solar energy as the primary source of power, US6977479B2, 2005. https://patents.google.com/patent/US6977479B2/en (accessed August 16, 2019).

[53] S. Niu, X. Wang, F. Yi, Y.S. Zhou, Z.L. Wang, A universal self-charging system driven by random biomechanical energy for sustainable operation of mobile electronics, Nature Communications. 6 (2015) 8975. https://doi.org/10.1038/ncomms9975.

[54] Y. Wang, Y. Yang, Z.L. Wang, Triboelectric nanogenerators as flexible power sources, Npj Flexible Electronics. 1 (2017) 10. https://doi.org/10.1038/s41528-017-0007-8.

[55] Y. Mao, N. Zhang, Y. Tang, M. Wang, M. Chao, E. Liang, A paper triboelectric nanogenerator for self-powered electronic systems, Nanoscale. 9 (2017) 14499–14505. https://doi.org/10.1039/C7NR05222G.

[56] X. Pu, L. Li, H. Song, C. Du, Z. Zhao, C. Jiang, G. Cao, W. Hu, Z.L. Wang, A Self-Charging Power Unit by Integration of a Textile Triboelectric Nanogenerator and a Flexible Lithium-Ion Battery for Wearable Electronics, Advanced Materials. 27 (2015) 2472–2478. https://doi.org/10.1002/adma.201500311.

[57] J. Wang, X. Li, Y. Zi, S. Wang, Z. Li, L. Zheng, F. Yi, S. Li, Z.L. Wang, A Flexible Fiber-Based Supercapacitor–Triboelectric-Nanogenerator Power System for Wearable Electronics, Advanced Materials. 27 (2015) 4830–4836. https://doi.org/10.1002/adma.201501934.

[58] W. Liu, Z. Wang, G. Wang, G. Liu, J. Chen, X. Pu, Y. Xi, X. Wang, H. Guo, C. Hu, Z.L. Wang, Integrated charge excitation triboelectric nanogenerator, Nature Communications. 10 (2019) 1426. https://doi.org/10.1038/s41467-019-09464-8.

[59] X. Wang, B. Yang, J. Liu, Y. Zhu, C. Yang, Q. He, A flexible triboelectric-piezoelectric hybrid nanogenerator based on P(VDF-TrFE) nanofibers and PDMS/MWCNT for wearable devices, Scientific Reports. 6 (2016) 36409. https://doi.org/10.1038/srep36409.

[60] J. Xiong, P. Cui, X. Chen, J. Wang, K. Parida, M.-F. Lin, P.S. Lee, Skin-touch-actuated textile-based triboelectric nanogenerator with black phosphorus for durable biomechanical energy harvesting, Nature Communications. 9 (2018) 4280. https://doi.org/10.1038/s41467-018-06759-0.

[61] G. Zhu, P. Bai, J. Chen, Z. Lin Wang, Power-generating shoe insole based on triboelectric nanogenerators for self-powered consumer electronics, Nano Energy. 2 (2013) 688–692. https://doi.org/10.1016/j.nanoen.2013.08.002.

[62] Y.H. Ko, G. Nagaraju, S.H. Lee, J.S. Yu, PDMS-based Triboelectric and Transparent Nanogenerators with ZnO Nanorod Arrays, ACS Appl. Mater. Interfaces. 6 (2014) 6631–6637. https://doi.org/10.1021/am5018072.

[63] F.-R. Fan, Z.-Q. Tian, Z. Lin Wang, Flexible triboelectric generator, Nano Energy. 1 (2012) 328–334. https://doi.org/10.1016/j.nanoen.2012.01.004.

[64] Q. Liang, X. Yan, Y. Gu, K. Zhang, M. Liang, S. Lu, X. Zheng, Y. Zhang, Highly transparent triboelectric nanogenerator for harvesting water-related energy reinforced by antireflection coating, Scientific Reports. 5 (2015) 9080. https://doi.org/10.1038/srep09080.

[65] Transparent Flexible Graphene Triboelectric Nanogenerators - Kim - 2014 - Advanced Materials - Wiley Online Library, (n.d.). https://onlinelibrary.wiley.com/doi/full/10.1002/adma.201400172 (accessed July 26, 2019).

[66] K.Y. Lee, M.K. Gupta, S.-W. Kim, Transparent flexible stretchable piezoelectric and triboelectric nanogenerators for powering portable electronics, Nano Energy. 14 (2015) 139–160. https://doi.org/10.1016/j.nanoen.2014.11.009.

[67] Y. Hwan Ko, S. Hyun Lee, J. Woo Leem, J. Su Yu, High transparency and triboelectric charge generation properties of nano-patterned PDMS, RSC Advances. 4 (2014) 10216–10220. https://doi.org/10.1039/C3RA47199C.

[68] B.N. Chandrashekar, B. Deng, A.S. Smitha, Y. Chen, C. Tan, H. Zhang, H. Peng, Z. Liu, Roll-to-Roll Green Transfer of CVD Graphene onto Plastic for a Transparent and Flexible Triboelectric Nanogenerator, Advanced Materials. 27 (2015) 5210–5216. https://doi.org/10.1002/adma.201502560.

[69] H. Guo, Q. Leng, X. He, M. Wang, J. Chen, C. Hu, Y. Xi, A Triboelectric Generator Based on Checker-Like Interdigital Electrodes with a Sandwiched PET Thin Film for Harvesting Sliding Energy in All Directions, Advanced Energy Materials. 5 (2015) 1400790. https://doi.org/10.1002/aenm.201400790.

[70] N. Kaur, J. Bahadur, V. Panwar, P. Singh, K. Rathi, K. Pal, Effective energy harvesting from a single electrode based triboelectric nanogenerator, Scientific Reports. 6 (2016) 38835. https://doi.org/10.1038/srep38835.

[71] Z.L. Wang, L. Lin, J. Chen, S. Niu, Y. Zi, Triboelectric Nanogenerator: Single-Electrode Mode, in: Z.L. Wang, L. Lin, J. Chen, S. Niu, Y. Zi (Eds.), Triboelectric Nanogenerators, Springer International Publishing, Cham, 2016: pp. 91–107. https://doi.org/10.1007/978-3-319-40039-6_4.

[72] S.W. Chen, X. Cao, N. Wang, L. Ma, H.R. Zhu, M. Willander, Y. Jie, Z.L. Wang, An Ultrathin Flexible Single-Electrode Triboelectric-Nanogenerator for Mechanical Energy Harvesting and Instantaneous Force Sensing, Advanced Energy Materials. 7 (2017) 1601255. https://doi.org/10.1002/aenm.201601255.

[73] K. Parida, V. Kumar, W. Jiangxin, V. Bhavanasi, R. Bendi, P.S. Lee, Highly Transparent, Stretchable, and Self-Healing Ionic-Skin Triboelectric Nanogenerators for Energy Harvesting and Touch Applications, Advanced Materials. 29 (2017) 1702181. https://doi.org/10.1002/adma.201702181.

[74] X. Wang, Y. Yin, F. Yi, K. Dai, S. Niu, Y. Han, Y. Zhang, Z. You, Bioinspired stretchable triboelectric nanogenerator as energy-harvesting skin for self-powered electronics, Nano Energy. 39 (2017) 429–436. https://doi.org/10.1016/j.nanoen.2017.07.022.

[75] Y. Yang, H. Zhang, Z.-H. Lin, Y.S. Zhou, Q. Jing, Y. Su, J. Yang, J. Chen, C. Hu, Z.L. Wang, Human Skin Based Triboelectric Nanogenerators for Harvesting Biomechanical Energy and as Self-Powered Active Tactile Sensor System, ACS Nano. 7 (2013) 9213–9222. https://doi.org/10.1021/nn403838y.

[76] T. Huang, C. Wang, H. Yu, H. Wang, Q. Zhang, M. Zhu, Human walking-driven wearable all-fiber triboelectric nanogenerator containing electrospun polyvinylidene fluoride piezoelectric nanofibers, Nano Energy. 14 (2015) 226–235. https://doi.org/10.1016/j.nanoen.2015.01.038.

[77] W. Yang, J. Chen, G. Zhu, J. Yang, P. Bai, Y. Su, Q. Jing, X. Cao, Z.L. Wang, Harvesting Energy from the Natural Vibration of Human Walking, ACS Nano. 7 (2013) 11317–11324. https://doi.org/10.1021/nn405175z.

[78] Y. Zi, J. Wang, S. Wang, S. Li, Z. Wen, H. Guo, Z.L. Wang, Effective energy storage from a triboelectric nanogenerator, Nature Communications. 7 (2016) 10987. https://doi.org/10.1038/ncomms10987.

[79] The Triboelectric Series - AlphaLab, Inc, AlphaLab, Inc. (n.d.). https://www.alphalabinc.com/triboelectric-series/ (accessed February 25, 2019).

[80] S. Rathore, S. Sharma, B.P. Swain, R.K. Ghadai, A Critical Review on Triboelectric Nanogenerator, IOP Conf. Ser.: Mater. Sci. Eng. 377 (2018) 012186. https://doi.org/10.1088/1757-899X/377/1/012186.

[81] M.A.P. Mahmud, N. Huda, S.H. Farjana, M. Asadnia, C. Lang, Recent Advances in Nanogenerator-Driven Self-Powered Implantable Biomedical Devices, Advanced Energy Materials. 8 (2018) 1701210. https://doi.org/10.1002/aenm.201701210.

[82] A.F. Diaz, R.M. Felix-Navarro, A semi-quantitative tribo-electric series for polymeric materials: the influence of chemical structure and properties, Journal of Electrostatics. 62 (2004) 277–290. https://doi.org/10.1016/j.elstat.2004.05.005.

[83] H. Zou, Y. Zhang, L. Guo, P. Wang, X. He, G. Dai, H. Zheng, C. Chen, A.C. Wang, C. Xu, Z.L. Wang, Quantifying the triboelectric series, Nature Communications. 10 (2019) 1–9. https://doi.org/10.1038/s41467-019-09461-x.

[84] H.-J. Yoon, H. Ryu, S.-W. Kim, Sustainable powering triboelectric nanogenerators: Approaches and the path towards efficient use, Nano Energy. 51 (2018) 270–285. https://doi.org/10.1016/j.nanoen.2018.06.075.

[85] W. Du, X. Han, L. Lin, M. Chen, X. Li, C. Pan, Z.L. Wang, A Three Dimensional Multi-Layered Sliding Triboelectric Nanogenerator, Advanced Energy Materials. 4 (2014) 1301592. https://doi.org/10.1002/aenm.201301592.

[86] X. Pu, M. Liu, X. Chen, J. Sun, C. Du, Y. Zhang, J. Zhai, W. Hu, Z.L. Wang, Ultrastretchable, transparent triboelectric nanogenerator as electronic skin for biomechanical energy harvesting and tactile sensing, Science Advances. 3 (2017) e1700015. https://doi.org/10.1126/sciadv.1700015.

[87] Dscout Research: people touch cellphones 2,617 times a day - Business Insider, (n.d.). https://www.businessinsider.com/dscout-research-people-touch-cell-phones-2617-times-a-day-2016-7 (accessed July 18, 2019).

[88] C.B. Crawford, B. Quinn, 4 - Physiochemical properties and degradation, in: C.B. Crawford, B. Quinn (Eds.), Microplastic Pollutants, Elsevier, 2017: pp. 57–100. https://doi.org/10.1016/B978-0-12-809406-8.00004-9.

[89] M. Leonhard, J. Lin, S. Huang, Touch screen protector, US8044942B1, 2011. https://patents.google.com/patent/US8044942B1/en (accessed July 21, 2019).

[90] J.Y. Lee, Y.S. Oh, H.J. PARK, S.H. Kim, Large-size touch screen, US20110216020A1, 2011. https://patents.google.com/patent/US20110216020A1/en (accessed July 21, 2019).

[91] H.-C. Hsieh, J.-Y. Chen, W.-Y. Lee, D. Bera, W.-C. Chen, Stretchable Fluorescent Polyfluorene/Acrylonitrile Butadiene Rubber Blend Electrospun Fibers through Physical Interaction and Geometrical Confinement, Macromolecular Rapid Communications. 39 (2018) 1700616. https://doi.org/10.1002/marc.201700616.

[92] T. Yasin, S. Ahmed, M. Ahmed, F. Yoshii, Effect of concentration of polyfunctional monomers on physical properties of acrylonitrile–butadiene rubber under electron-beam irradiation, Radiation Physics and Chemistry. 73 (2005) 155–158. https://doi.org/10.1016/j.radphyschem.2004.07.009.

[93] J.-M. Andanson, S.G. Kazarian, In situ ATR-FTIR Spectroscopy of Poly(ethylene terephthalate) Subjected to High-Temperature Methanol, Macromol. Symp. 265 (2008) 195–204. https://doi.org/10.1002/masy.200850521.

[94] M. Mecozzi, L. Nisini, The differentiation of biodegradable and non-biodegradable polyethylene terephthalate (PET) samples by FTIR spectroscopy: A potential support for the structural differentiation of PET in environmental analysis, Infrared Physics & Technology. 101 (2019) 119–126. https://doi.org/10.1016/j.infrared.2019.06.008.

[95] K. Elnagar, T. Abou Elmaaty, S. Raouf, Dyeing of Polyester and Polyamide Synthetic Fabrics with Natural Dyes Using Ecofriendly Technique, Journal of Textiles. (2014). https://doi.org/10.1155/2014/363079.

[96] A. a. M. El-Saftawy, Regulating The Performance Parameters Of Accelerated Particles, (2013). http://inis.iaea.org/Search/search.aspx?orig_q=RN:46135147 (accessed July 25, 2019).

[97] S. Samantarai, A. Nag, N. Singh, D. Dash, A. Basak, G.B. Nando, N.C. Das, Chemical modification of nitrile rubber in the latex stage by functionalizing phosphorylated cardanol prepolymer: A bio-based plasticizer and a renewable resource, Journal of Elastomers & Plastics. 51 (2019) 99–129. https://doi.org/10.1177/0095244318768644.

[98] A. Alhareb, H. Akil, Z. Ahmad, Poly(methyl methacrylate) denture base composites enhancement by various combinations of nitrile butadiene rubber/treated ceramic fillers, Journal of Thermoplastic Composite Materials. 30 (2017) 1069–1090. https://doi.org/10.1177/0892705715616856.

[99] Y. Zou, P. Tan, B. Shi, H. Ouyang, D. Jiang, Z. Liu, H. Li, M. Yu, C. Wang, X. Qu, L. Zhao, Y. Fan, Z.L. Wang, Z. Li, A bionic stretchable nanogenerator for underwater sensing and energy harvesting, Nature Communications. 10 (2019) 2695. https://doi.org/10.1038/s41467-019-10433-4.

[100] L. Gu, N. Cui, L. Cheng, Q. Xu, S. Bai, M. Yuan, W. Wu, J. Liu, Y. Zhao, F. Ma, Y. Qin, Z.L. Wang, Flexible Fiber Nanogenerator with 209 V Output Voltage Directly Powers a Light-Emitting Diode, Nano Lett. 13 (2013) 91–94. https://doi.org/10.1021/nl303539c.

[101] X. Wang, B. Yang, J. Liu, Y. Zhu, C. Yang, Q. He, A flexible triboelectric-piezoelectric hybrid nanogenerator based on P(VDF-TrFE) nanofibers and PDMS/MWCNT for wearable devices, Scientific Reports. 6 (2016) 36409. https://doi.org/10.1038/srep36409.

[102] M. Murai, H.-K. Lau, B.P. Pereira, R.W.H. Pho, A cadaver study on volume and surface area of the fingertip, The Journal of Hand Surgery. 22 (1997) 935–941. https://doi.org/10.1016/S0363-5023(97)80094-9.

[103] K. Parida, G. Thangavel, G. Cai, X. Zhou, S. Park, J. Xiong, P.S. Lee, Extremely stretchable and self-healing conductor based on thermoplastic elastomer for all-three-dimensional printed triboelectric nanogenerator, Nature Communications. 10 (2019) 2158. https://doi.org/10.1038/s41467-019-10061-y.

[104] M. Ma, Z. Kang, Q. Liao, Q. Zhang, F. Gao, X. Zhao, Z. Zhang, Y. Zhang, Development, applications, and future directions of triboelectric nanogenerators, Nano Res. 11 (2018) 2951–2969. https://doi.org/10.1007/s12274-018-1997-9.

[105] C. Ramon, P. Garguilo, E.A. Fridgeirsson, J. Haueisen, Changes in scalp potentials and spatial smoothing effects of inclusion of dura layer in human head models for EEG simulations, Front Neuroeng. 7 (2014). https://doi.org/10.3389/fneng.2014.00032.

[106] A. Boonbumrung, P. Sae-oui, C. Sirisinha, Reinforcement of Multiwalled Carbon Nanotube in Nitrile Rubber: In Comparison with Carbon Black, Conductive Carbon Black, and Precipitated Silica, Journal of Nanomaterials. (2016). https://doi.org/10.1155/2016/6391572.

[107] Y. Zhu, B. Yang, J. Liu, X. Wang, L. Wang, X. Chen, C. Yang, A flexible and biocompatible triboelectric nanogenerator with tunable internal resistance for powering wearable devices, Scientific Reports. 6 (2016) 22233. https://doi.org/10.1038/srep22233.

[108] G. Hassan, F. Khan, A. Hassan, S. Ali, J. Bae, C.H. Lee, A flat-panel-shaped hybrid piezo/triboelectric nanogenerator for ambient energy harvesting, Nanotechnology. 28 (2017) 175402. https://doi.org/10.1088/1361-6528/aa65c3.

[109] H. Zhang, Y. Yang, T.-C. Hou, Y. Su, C. Hu, Z.L. Wang, Triboelectric nanogenerator built inside clothes for self-powered glucose biosensors, Nano Energy. 2 (2013) 1019–1024. https://doi.org/10.1016/j.nanoen.2013.03.024.

[110] D. Yoo, E.Y. Go, D. Choi, J.-W. Lee, I. Song, J.-Y. Sim, W. Hwang, D.S. Kim, Increased Interfacial Area between Dielectric Layer and Electrode of Triboelectric Nanogenerator toward Robustness and Boosted Energy Output, Nanomaterials. 9 (2019) 71. https://doi.org/10.3390/nano9010071.

[111] C. Cui, X. Wang, Z. Yi, B. Yang, X. Wang, X. Chen, J. Liu, C. Yang, Flexible Single-Electrode Triboelectric Nanogenerator and Body Moving Sensor Based on Porous Na2CO3/Polydimethylsiloxane Film, ACS Appl. Mater. Interfaces. 10 (2018) 3652–3659. https://doi.org/10.1021/acsami.7b17585.

[112] X. Hu, S. Li, H. Peng, A comparative study of equivalent circuit models for Li-ion batteries, Journal of Power Sources. 198 (2012) 359–367. https://doi.org/10.1016/j.jpowsour.2011.10.013.

[113] L. Lu, X. Han, J. Li, J. Hua, M. Ouyang, A review on the key issues for lithium-ion battery management in electric vehicles, Journal of Power Sources. 226 (2013) 272–288. https://doi.org/10.1016/j.jpowsour.2012.10.060.

[114] E.R. Delay, A.J. Golden, N.O. Steiner, A compact IC tone generator, Physiology & Behavior. 21 (1978) 133–134. https://doi.org/10.1016/0031-9384(78)90288-3.

[115] G. Zhu, Z.-H. Lin, Q. Jing, P. Bai, C. Pan, Y. Yang, Y. Zhou, Z.L. Wang, Toward Large-Scale Energy Harvesting by a Nanoparticle-Enhanced Triboelectric Nanogenerator, Nano Lett. 13 (2013) 847–853. https://doi.org/10.1021/nl4001053.

[116] M. Tsuji, S. Hikino, R. Tanabe, Y. Sano, Synthesis of Bicompartmental Ag/Cu Nanoparticles Using a Two-step Polyol Process, Chem. Lett. 38 (2009) 860–861. https://doi.org/10.1246/cl.2009.860.

[117] T. Shen, Y. Liu, Y. Zhu, D.-Q. Yang, E. Sacher, Improved adhesion of Ag NPs to the polyethylene terephthalate surface via atmospheric plasma treatment and surface functionalization, Applied Surface Science. 411 (2017) 411–418. https://doi.org/10.1016/j.apsusc.2017.03.149.

[118] J.A. Adekoya, E.O. Dare, M.A. Mesubi, Tunable morphological properties of silver enriched platinum allied nanoparticles and their catalysed reduction of p-nitrophenol, Adv. Nat. Sci: Nanosci. Nanotechnol. 5 (2014) 035007. https://doi.org/10.1088/2043-6262/5/3/035007.

[119] J. Hao, Z. Xu, R. Chu, Y. Zhang, Q. Chen, P. Fu, W. Li, G. Li, Q. Yin, Characterization of (K0.5Na0.5)NbO3 powders and ceramics prepared by a novel hybrid method of sol–gel and ultrasonic atomization, Materials & Design. 31 (2010) 3146–3150. https://doi.org/10.1016/j.matdes.2009.12.015.

[120] Q. Chai, X. Zhao, X. Chao, Z. Yang, Enhanced transmittance and piezoelectricity of transparent $K_{0.5}Na_{0.5}NbO_3$ ceramics with $Ca(Zn_{1/3}Nb_{2/3})O_3$ additives, RSC Adv. 7 (2017) 28428–28437. https://doi.org/10.1039/C7RA04064D.

[121] Gh.H. Khorrami, A. Kompany, A. Khorsand Zak, A facile sol–gel approach to synthesize KNN nanoparticles at low temperature, Materials Letters. 110 (2013) 172–175. https://doi.org/10.1016/j.matlet.2013.07.115.

[122] Y. Zhao, Y. Chen, K. Chen, Improvement in synthesis of (K0.5Na0.5)NbO3 powders by Ge4+ acceptor doping, Front. Mater. Sci. 10 (2016) 422–427. https://doi.org/10.1007/s11706-016-0362-8.

[123] R. Sierra-Ávila, M. Pérez-Alvarez, G. Cadenas-Pliego, V. Comparán Padilla, C. Ávila-Orta, O. Pérez Camacho, E. Jiménez-Regalado, E. Hernández-Hernández, R.M. Jiménez-Barrera, Synthesis of Copper Nanoparticles Using Mixture of Allylamine and Polyallylamine, Journal of Nanomaterials. (2015). https://doi.org/10.1155/2015/367341.

[124] Y. Yong, T. Yonezawa, M. Matsubara, H. Tsukamoto, The mechanism of alkylamine-stabilized copper fine particles towards improving the electrical conductivity of copper films at low sintering temperature, Journal of Materials Chemistry C. 3 (2015) 5890–5895. https://doi.org/10.1039/C5TC00745C.

[125] Y.-J. Kim, C.H. Ahn, M.B. Lee, M.-S. Choi, Characteristics of electrospun PVDF/SiO2 composite nanofiber membranes as polymer electrolyte, Materials Chemistry and Physics. 127 (2011) 137–142. https://doi.org/10.1016/j.matchemphys.2011.01.046.

[126] S. Janakiraman, A. Surendran, S. Ghosh, S. Anandhan, A. Venimadhav, Electroactive poly(vinylidene fluoride) fluoride separator for sodium ion battery with high coulombic efficiency, Solid State Ionics. 292 (2016) 130–135. https://doi.org/10.1016/j.ssi.2016.05.020.

[127] X. Cai, T. Lei, D. Sun, L. Lin, A critical analysis of the α, β and γ phases in poly(vinylidene fluoride) using FTIR, RSC Adv. 7 (2017) 15382–15389. https://doi.org/10.1039/C7RA01267E.

[128] W.A. Yee, M. Kotaki, Y. Liu, X. Lu, Morphology, polymorphism behavior and molecular orientation of electrospun poly(vinylidene fluoride) fibers, Polymer. 48 (2007) 512–521. https://doi.org/10.1016/j.polymer.2006.11.036.

[129] S.K. Karan, D. Mandal, B.B. Khatua, Self-powered flexible Fe-doped RGO/PVDF nanocomposite: an excellent material for a piezoelectric energy harvester, Nanoscale. 7 (2015) 10655–10666. https://doi.org/10.1039/C5NR02067K.

[130] M. Li, N. Stingelin, J.J. Michels, M.-J. Spijkman, K. Asadi, K. Feldman, P.W.M. Blom, D.M. de Leeuw, Ferroelectric Phase Diagram of PVDF:PMMA, Macromolecules. 45 (2012) 7477–7485. https://doi.org/10.1021/ma301460h.

[131] J. Yang, H. Chen, Z. Wang, Synthesis of sodium-potassium niobate (K, Na)NbO3 lead-free piezoelectric powders using solvothermal and hydrothermal processing, in: Proceedings of the 2010 Symposium on Piezoelectricity, Acoustic Waves and Device Applications, IEEE, Xiamen, China, 2010: pp. 249–253. https://doi.org/10.1109/SPAWDA.2010.5744314.

[132] M. Feizpour, H. Barzegar Bafrooei, R. Hayati, T. Ebadzadeh, Microwave-assisted synthesis and sintering of potassium sodium niobate lead-free piezoelectric ceramics, Ceramics International. 40 (2014) 871–877. https://doi.org/10.1016/j.ceramint.2013.06.081.

[133] C. Wang, Y. Hou, H. Ge, M. Zhu, H. Wang, H. Yan, Sol–gel synthesis and characterization of lead-free LNKN nanocrystalline powder, Journal of Crystal Growth. 310 (2008) 4635–4639. https://doi.org/10.1016/j.jcrysgro.2008.08.042.

[134] M. del C.B. López, G. Fourlaris, B. Rand, F.L. Riley, Characterization of Barium Titanate Powders: Barium Carbonate Identification, Journal of the American Ceramic Society. 82 (1999) 1777–1786. https://doi.org/10.1111/j.1151-2916.1999.tb01999.x.

[135] H. Parangusan, D. Ponnamma, M.A.A. Al-Maadeed, Stretchable Electrospun PVDF-HFP/Co-ZnO Nanofibers as Piezoelectric Nanogenerators, Scientific Reports. 8 (2018) 754. https://doi.org/10.1038/s41598-017-19082-3.

[136] J.-H. Lee, H.-J. Yoon, T.Y. Kim, M.K. Gupta, J.H. Lee, W. Seung, H. Ryu, S.-W. Kim, Micropatterned P(VDF-TrFE) Film-Based Piezoelectric Nanogenerators for Highly Sensitive Self-Powered Pressure Sensors, Advanced Functional Materials. 25 (2015) 3203–3209. https://doi.org/10.1002/adfm.201500856.

[137] A.R. Chowdhury, J. Jaksik, I. Hussain, R. Longoria, O. Faruque, F. Cesano, D. Scarano, J. Parsons, M.J. Uddin, Multicomponent nanostructured materials and interfaces for efficient piezoelectricity, Nano-Structures & Nano-Objects. 17 (2019) 148–184. https://doi.org/10.1016/j.nanoso.2018.12.002.

[138] S.Y. Chung, S. Kim, J.-H. Lee, K. Kim, S.-W. Kim, C.-Y. Kang, S.-J. Yoon, Y.S. Kim, All-Solution-Processed Flexible Thin Film Piezoelectric Nanogenerator, Advanced Materials. 24 (2012) 6022–6027. https://doi.org/10.1002/adma.201202708.

[139] G. Suo, Y. Yu, Z. Zhang, S. Wang, P. Zhao, J. Li, X. Wang, Piezoelectric and Triboelectric Dual Effects in Mechanical-Energy Harvesting Using BaTiO3/Polydimethylsiloxane Composite Film, ACS Appl. Mater. Interfaces. 8 (2016) 34335–34341. https://doi.org/10.1021/acsami.6b11108.

[140] G. Liu, E. Abdel-Rahman, D. Ban, Performance optimization of p-n homojunction nanowire-based piezoelectric nanogenerators through control of doping concentration, Journal of Applied Physics. 118 (2015) 094307. https://doi.org/10.1063/1.4930031.

[141] Y. Sun, J. Chen, X. Li, Y. Lu, S. Zhang, Z. Cheng, Flexible piezoelectric energy harvester/sensor with high voltage output over wide temperature range, Nano Energy. 61 (2019) 337–345. https://doi.org/10.1016/j.nanoen.2019.04.055.

[142] D. Giovanelli, E. Farella, Force Sensing Resistor and Evaluation of Technology for Wearable Body Pressure Sensing, Journal of Sensors. 2016 (2016) e9391850. https://doi.org/10.1155/2016/9391850.

[143] F. Reza, G.B. Batson, J.A. Yamamuro, J.S. Lee, Resistance Changes during Compression of Carbon Fiber Cement Composites, Journal of Materials in Civil Engineering. 15 (2003) 476–483. https://doi.org/10.1061/(ASCE)0899-1561(2003)15:5(476).

[144] S. Bairagi, S.W. Ali, A unique piezoelectric nanogenerator composed of melt-spun PVDF/KNN nanorod-based nanocomposite fibre, European Polymer Journal. 116 (2019) 554–561. https://doi.org/10.1016/j.eurpolymj.2019.04.043.

[145] G. Zhao, X. Zhang, X. Cui, S. Wang, Z. Liu, L. Deng, A. Qi, X. Qiao, L. Li, C. Pan, Y. Zhang, L. Li, Piezoelectric Polyacrylonitrile Nanofiber Film-Based Dual-Function Self-Powered Flexible Sensor, ACS Appl. Mater. Interfaces. 10 (2018) 15855–15863. https://doi.org/10.1021/acsami.8b02564.

[146] J. He, S. Qian, X. Niu, N. Zhang, J. Qian, X. Hou, J. Mu, W. Geng, X. Chou, Piezoelectric-enhanced triboelectric nanogenerator fabric for biomechanical energy harvesting, Nano Energy. 64 (2019) 103933. https://doi.org/10.1016/j.nanoen.2019.103933.

[147] A. Proto, M. Penhaker, S. Conforto, M. Schmid, Nanogenerators for Human Body Energy Harvesting, Trends in Biotechnology. 35 (2017) 610–624. https://doi.org/10.1016/j.tibtech.2017.04.005.

[148] A. Yu, P. Jiang, Z. Lin Wang, Nanogenerator as self-powered vibration sensor, Nano Energy. 1 (2012) 418–423. https://doi.org/10.1016/j.nanoen.2011.12.006.

[149] M.I. Friswell, S. Adhikari, Sensor shape design for piezoelectric cantilever beams to harvest vibration energy, Journal of Applied Physics. 108 (2010) 014901. https://doi.org/10.1063/1.3457330.

[150] J. Ajitsaria, S.Y. Choe, D. Shen, D.J. Kim, Modeling and analysis of a bimorph piezoelectric cantilever beam for voltage generation, Smart Mater. Struct. 16 (2007) 447–454. https://doi.org/10.1088/0964-1726/16/2/024.

[151] A.M. Abdullah, A. Flores, A.R. Chowdhury, J. Li, Y. Mao, M.J. Uddin, Synthesis and fabrication of self-sustainable triboelectric energy case for powering smart electronic devices, Nano Energy. (2020) 104774. https://doi.org/10.1016/j.nanoen.2020.104774.

[152] J.P. Lee, J.W. Lee, J.M. Baik, The Progress of PVDF as a Functional Material for Triboelectric Nanogenerators and Self-Powered Sensors, Micromachines (Basel). 9 (2018). https://doi.org/10.3390/mi9100532.

[153] S. Cheon, H. Kang, H. Kim, Y. Son, J.Y. Lee, H.-J. Shin, S.-W. Kim, J.H. Cho, High-Performance Triboelectric Nanogenerators Based on Electrospun Polyvinylidene Fluoride–Silver Nanowire Composite Nanofibers, Advanced Functional Materials. 28 (2018) 1703778. https://doi.org/10.1002/adfm.201703778.

[154] X.-S. Zhang, M.-D. Han, R.-X. Wang, F.-Y. Zhu, Z.-H. Li, W. Wang, H.-X. Zhang, Frequency-Multiplication High-Output Triboelectric Nanogenerator for Sustainably

Powering Biomedical Microsystems, Nano Lett. 13 (2013) 1168–1172. https://doi.org/10.1021/nl3045684.

[155] Y. Yao, T. Jiang, L. Zhang, X. Chen, Z. Gao, Z.L. Wang, Charging System Optimization of Triboelectric Nanogenerator for Water Wave Energy Harvesting and Storage, ACS Appl. Mater. Interfaces. 8 (2016) 21398–21406. https://doi.org/10.1021/acsami.6b07697.

[156] K. Zhao, Y. Wang, L. Han, Y. Wang, X. Luo, Z. Zhang, Y. Yang, Nanogenerator-Based Self-Charging Energy Storage Devices, Nano-Micro Lett. 11 (2019) 19. https://doi.org/10.1007/s40820-019-0251-7.

[157] Y. Wang, Y. Yang, Z.L. Wang, Triboelectric nanogenerators as flexible power sources, Npj Flexible Electronics. 1 (2017) 1–10. https://doi.org/10.1038/s41528-017-0007-8.

[158] K. Liu, T. Ding, J. Li, Q. Chen, G. Xue, P. Yang, M. Xu, Z.L. Wang, J. Zhou, Thermal–Electric Nanogenerator Based on the Electrokinetic Effect in Porous Carbon Film, Advanced Energy Materials. 8 (2018) 1702481. https://doi.org/10.1002/aenm.201702481.

[159] F.-R. Fan, Z.-Q. Tian, Z. Lin Wang, Flexible triboelectric generator, Nano Energy. 1 (2012) 328–334. https://doi.org/10.1016/j.nanoen.2012.01.004.

[160] R.K. Cheedarala, J.I. Song, Sand-polished Kapton film and aluminum as source of electron transfer triboelectric nanogenerator through vertical contact separation mode, International Journal of Smart and Nano Materials. 11 (2020) 38–46. https://doi.org/10.1080/19475411.2020.1727991.

BIOGRAPHICAL SKETCH

Abu Musa Abdullah has completed his BSc in Mechanical Engineering from Bangladesh University of Engineering in 2017. He joined at the department of Mechanical Engineering at the University of Texas Rio Grande Valley on 2018. Since then, he had been working at the Photonics and Energy Research Laboratory under the supervision of Dr. M. Jasim Uddin. He had also worked as Graduate Teaching Assistant under Dr. Horacio Vasquez. He earned his Master of Science in Engineering degree from the University of Texas Rio Grande Valley on August 2020. His research interest mainly focuses on Nanomaterials for Energy Harvesting, Piezoelectric and Triboelectric Materials, Renewable Energy Systems, Nanoengineered Devices and Sensors and Multifunctional Composite Materials. He has received the prestigious Presidential Graduate Research Assistantship (2018-2020), 1st Runner up at the Graduate Research Showcase (Fall 2019) and High Scholar Award (First Prize Co-mentor). So far, he has published 5 journal articles in prestigious journals and at least 5 more are underway. He is expected to join Pennsylvania State University on Fall 2020 for PhD in Engineering Science and Mechanics in Materials concentration under the Materials Research Institute. He can be reached at abdullahshourav11@gmail.com.